國立交通大學
材料科學與工程學研究所
碩 士 論 文

利用奈米壓痕機量測 BOAC(Bonding Pad Over Active Circuits)結構的機械強度和接合性

Evaluation of Mechanical Strength and Bondability of BOAC (Bonding Pad Over Active Circuits) Structures using Nanoindentation

研 究 生：湯季高

指導教授：呂志鵬　教授

中 華 民 國 九十六 年 八 月

利用奈米壓痕機量測 BOAC(Bonding Pad Over Active Circuits)結構的機械強度和接合性

Evaluation of Mechanical Strength and Bondability of BOAC (Bonding Pad Over Active Circuits) Structures using Nanoindentation

研 究 生：湯季高　　Student：Chi-Kao Tang

指導教授：呂志鵬　　Advisor：Dr. Jihperng (Jim) Leu

國 立 交 通 大 學

材 料 科 學 與 工 程 學 系

碩 士 論 文

A Thesis

Submitted to Department of Materials Science and Engineering

College of Engineering

National Chiao Tung University

in partial Fulfillment of the Requirements

for the Degree of

Master

in

Materials Science and Engineering

August 2007

Hsinchu, Taiwan, Republic of China

中華民國九十六年八月

利用奈米壓痕機量測 BOAC(Bonding Pad Over Active Circuits)結構的機械強度和接合性

學生: 湯季高　　指導教授:呂志鵬 教授

國立交通大學材料與工程學系碩士班

摘要

本論文著重於建立一套利用奈米壓痕機量測 BOAC 銲墊下結構機械抵抗力的方法，以準確預測 BOAC 接合性及改善開發時效。本研究利用基材效應來判別不同 BOAC 結構的機械強度，並利用 King's 方程式回歸實驗數據以量化所有 BOAC 結構的機械強度。從實驗的結果，我們成功的利用基材效應計算出 4 種不同影響因素對 BOAC 機械強度的影響，分別為(1) 銲墊結構: 具高金屬密度及 trench/via 堆疊的傳統銲墊比 BOAC 強。(2) 銅導線密度: 最上金屬層的密度對整體 BOAC 強度的影響不大，表示最上層的鋁和 oxide 吸收了大部分的衝擊力量而保護了下面的結構免受壓痕的衝擊。(3) 線寬尺寸: 65 nm 在銅/介電層中，銅的比例比 90 nm 的高，導致整體 BOAC 的強度較 90 nm 的強。(4) 低介電材料: 此因素對整體 BOAC 強度的影響最大，從實驗結果及斷面的觀察中可知其影響因素應為低彈性係數及低介面附著力所導致整體機械強度的弱化。總括而言，我們可以(1) 在銅/介電層中，增加銅的比例，(2) 使用彈性係數及介面附著力較佳的低介電材料，(3) 在 BOAC 結構的上層增加強度較佳的保護層以增強 BOAC 結構的機械強度。

本研究並使用兩種不同膜/基材的系統: (1) 鋁/均勻基材(軟膜/硬基材)和(2) oxide/均勻基材(硬膜/軟基材)來比較 King's 方程式量化的結果在此兩種系統中之適用性與差異性。實驗結果發現不同 BOAC 結構機械強度的大小趨勢在此兩種系統中是相同的，但是受到基材硬度的影響，量化的值在鋁/均勻基材系統中是

被高估，而在 Oxide/均勻基材系統中是被低估。甚至，我們在 Oxide/均勻基材系統中發現基材的影響範圍是會隨著壓痕的深度而持續往下的。

吾人利用P/S^2這項函數將硬度的效應去除，反推BOAC結構真實的機械強度變化，發現BOAC基材並不是呈現一個單一的均勻基材，而是呈現出一個隨著壓痕深度持續改變的多層基材。利用此實驗方法所估算出oxide下基材的機械強度與利用複合材料理論計算出的值大小趨勢是一致的，且與King's方程式的量化值相比，P/S^2估算出的值與複合材料理論的值更為吻合。利用此方法更能了解BOAC結構機械強度的變化。總括以上的討論，我們成功的以簡化之King's方程式與P/S^2方法估算BOAC的機械強度，而在King's方程式量化的值中，吾人推論其BOAC的複合彈性模數至少應具 70 GPa方可確保通過接合性的測試。

Evaluation of Mechanical Strength and Bondability of BOAC (Bonding Pad Over Active Circuits) Structures using Nanoindentation

Student: Chi-Kao Tang Advisors: Dr. Jihperng (Jim) Leu

Department of Material Science and Engineering

National Chiao Tung University

Abstract

The aim of this thesis was to establish a novel methodology using nanoindentation, which stimulated wire bonding and probing, to distinguish the mechanical resistance of various bonding pad-over-active-circuits (BOAC) structures by means of substrate effect. Such a quick turn-around methodology was also intended for predicting the bondability without a full array of reliability tests to reduce R&D cycle time. The mechanical stiffness of BOAC structures can be quantified using King's model to fit the nanoindentation results assuming a uniform two-layered Al or oxide/substrate system. The parameters affecting the mechanical strength of BOAC such as bond pad types, copper density, line width/pitch (technology nodes) and low-k dielectric materials were investigated in this thesis to identify general design rules for BOAC layouts and structures. From nanoindentation results, normal pad was found to be much stronger than BOAC pad because normal pad had full stack of trench/via dummification. In addition, the top copper metal's density had little

influence on mechanical strength of BOAC structures because the top layers such as Al and oxide layer absorbed the majority of impact force; thus provided good protection for the structures underneath Al/oxide layers. When the metal line widths and pitches scaled from 90 nm to 65 nm process node, the BOAC became stronger because 65nm had higher copper fraction in Cu/low-k layer. The type of low-k materials was found to have great influence in the mechanical strength of BOAC structures. In summary, BOAC structures can be strengthened by (1) increasing aspect ratio (AR) in Cu/low-k layer, (2) using low-k materials with better modulus and interfacial adhesion, and (3) adding a stronger buffer layer such as oxide layer on the top of BOAC structures.

In this study, two different film/substrate systems, *i.e.* (1) Al/composite substrate (soft film/hard substrate system) and (2) oxide/composite substrate (hard film/soft substrate system) were also examined to assess the applicability of fitting method using King's model. The tendency of mechanical strength in different BOAC structures was found to be the same in these two different film/substrate systems. However, the quantified values were overestimated in Al/composite substrate, but underestimated in oxide/composite substrate due to the substrate hardness effect.

Then, P/S^2 term was used to eliminate the substrate hardness effect. The results truthfully showed a varying multilayered substrate with increasing indenter depth. This method could be used to analyze the changing mechanical strength of multilayer in BOAC structures as a function of indenter depth. The P/S^2 results showed not only the same tendency of mechanical strength as that of theoretical calculation using the equation of composite materials, but also smaller deviation from theoretical calculation, as compared to values obtained from King's model fitting. Overall, a novel methodology based on nanoindentation has been successfully established to distinguish the mechanical strength of various BOAC structures through a composite

modulus values using a simplified film/uniform substrate model or P/S^2 model. In addition, a modulus of 70 GPa in composite substrate of bond pad structure can be considered as a sufficient condition for new BOAC layouts passing the bondability tests.

Acknowledgements

很開心終於完成我的碩士論文，回想待在交通大學的四年大學生涯，以及兩年的研究所生活，有很多汗水和淚水，但是有更多美麗的回憶和笑容，這六年的生活及訓練，把我從一個懵懵懂懂的傻小子，變成一個勇敢接受未來挑戰的新鮮人，其中有太多人在背後默默支持我、幫助我，在此我將獻上我最大的感激。

首先我要謝謝NIP實驗室的大家長，也就是我的指導教授呂志鵬老師，當初很幸運的加入這個團隊，老師總是不斷的在實驗上以及生活上給我鼓勵以及指導，讓我這兩年研究所生涯雖然可以說是風浪不斷，但老師點了那盞明燈，總是可以讓我知道靠岸的航線，在此我要說聲謝謝您，老師。

另外感謝國科會(計畫編號:NSC95-2221-E009-309)與 SRC/UMC(計畫編號:1301.001)於實驗經費的贊助，以及感謝聯華電子(UMC)的陳國明經理與吳炳昌先生等人大力的協助，因為有你們的體諒及幫忙，使得本論文能夠更完整而嚴謹，沒有你們支持這個計畫的推動，我是沒有辦法順利完成我的論文的。

接著我要感謝實驗室的同窗好友們，謝謝國原學長在我的實驗與生活的過程中，不斷地給我提醒及幫忙，尤其在我死腦筋的時候，真是惠我良多。謝謝昱涵學長總是陪我熬夜做實驗，還講笑話給我聽，您人真好。謝謝牧龍學長，你就像我的兄長一樣，在生活上總是給我最多的支持，謝謝你!還要感謝明義、泰印、志安、元辰、子豪學長以及幸鈴學姐不厭其煩的指出我研究中的缺失，且總能在我迷惘時為我解惑。特別感謝Gary學長在儀器組裝上給予的幫助。最後要謝謝同窗好友陪我一起走過這兩年，謝謝冠宇、鈞元、欣源同學，一起度過了無數個熬夜讀書、趕作業以及打怪練功的夜晚，沒有你們，我的生活不會這麼多采多姿的。實驗室的王智、少農、傑哥學弟、怡臻學妹當然也不能忘記，你們的幫忙及搞笑我銘感在心。

最後，謹以此文獻給我摯愛的雙親。

Contents

List of Tables

List of Figures

Chapter 1 Introduction

The performance of IC device technology continued its advancement in speed as the minimum feature of transistor scaled at 30 % every 18 months according to Moore's law [1]. However, taking advantage of the cost reduction per transistor from device scaling, designers put more functions and complexity in the chips, which required proportionally larger numbers of I/O connection. For conventional wire-bonding packaging, typically bond pad was located outside of active circuitry area and was fabricated by adding a top metal layer [2] under which several design rules such as EDS protection and test key were added. As I/O increased, the peripheral area defined by bond pads dictated the die size instead of the active circuitry. One approach of alleviating such problem was to use tighter bond pad sizes and pitches, but this was constrained by the wire bonding capability. Excluding a switch to more costly flip-chip package through solder bumping, wire bonding pads over active circuit (BOAC) was a viable alternative, which could relax the constraints on bond pad size and pitch and also reduce the die size. Moreover, on-chip bussing and interconnect resistance could be reduced because the bond pads was located closer to the active circuit [3]. However, unlike the conventional normal pads which had better protection with mechanical support by underlying dummified trench/via structures, the reliability of BOAC during the fabrication, probing and wire bonding process was of great concern because poor mechanical support would cause mechanical damage such as delamination and cracks or devices failure. As low-dielectric-constant (low-k) or ultra low-k dielectric was introduced into backend interconnect to reduce RC delay, the evaluation and reliability test of BOAC layout technology for Cu/low-k structures underneath bonding pads were imperative and even challenging because the mechanical properties of these low-k materials were

very weak, approximately 7-10 times lower than the SiO_2 [4-5].

Although modeling [6-7] had been employed to understand the stress impact to the wire bonding process and BOAC structures, limited success was achieved in the improvement of mechanical reliability of BOAC structures. Still, there was no change in the test methodology and development cycle time. It was highly desirable to develop a novel experimental methodology to accelerate the evaluation of various BOAC layout designs for copper/low-k backend interconnects without a full array of reliability tests in early development stage.

In this thesis, nanoindentation was proposed as a quick turn-around methodology because the down force of nanoindentation was similar to that of wire bonding process (down force of 5~25 mN). In this thesis, nanoindentation was used to simulate the impact force of wire bonding or wafer probing in the packaging process and testing steps. Based on nanoindentation measurements, the mechanical resistance of different BOAC structures can be evaluated. In addition, the mechanical strength of BOAC structures can be quantified using a uniform two-layered model such as King's model and a model taking contact area into account.

Two different BOAC stacks were investigated in this thesis. The first BOAC structure was Al/composite substrate system which could be categorized as a soft film/hard substrate system. The other BOAC structure was oxide/composite substrate system which could be categorized as a hard film/soft substrate system. The objective is to cross-check the fitting results and to understand any difference of the values obtained from nanoindentation method.

This thesis includes: (1) Chapter 1 on Introduction, (2) Chapter 2 on Literature review and Motivations, (3) Chapter 3 on Experimental methods, (4) Chapter 4 on Results and Discussion, (5) Chapter 5 on Conclusions.

Chapter 2 Literature Review and Motivations

2.1 Introduction of IC packaging

The IC packaging covers all the processes of sealing, fastening and connection etc. in an integrated circuit chip. The main purposes of packaging are [8]:

(1) Transmission of power

(2) Transmission of signal

(3) Heat dissipation

(4) Circuit protecting and supporting

For the signal transmission, there are three main techniques to provide IC chip signal connection between chip and substrate [9]: wire bonding, tape automated bonding (TAB), and flip chip (FC). The comparison of these methods and the technology roadmap of wire bond and flip chip technology [10] are outlined in Tables 2.1 and 2.2. Flip chip packaging has the most I/O numbers and it becomes more important in high-level IC products. Although wire bond has less I/O numbers, it still has the advantages of lower cost and mature process. In low-level products, the functions are not so complicated that do not need many I/O numbers. Therefore wire bonding is still the most popular method in packaging. Nevertheless the bond pad pitch will continue scaling down, the impact force per unit area will increase; thus may pose challenge on the mechanical reliability. In the next section, wire bonding process and its challenges will be further reviewed in details.

Table 2.1 Comparison of wire bond, TAB, and flip chip packaging [6]

	Wire bond	TAB	Flip chip
Area ratio	1	1.33	0.33
Weight ratio	1	0.25	0.2
Thickness ratio	1	0.67	0.52
I/O numbers	300~500	500~700	>1000
Bond pad pitch	~50 μm	40 μm	~150 μm
Ball size	~40 μm	NA	~150 μm
Interval of bond pad	100~180 μm	80 μm	~300 μm

Table 2.2 2006 ITRS report: Roadmaps of wire bond and flip chip packaging [10]

	2005	2006	2007	2008	2009	2010	2011	2012	2013
Pad pitch Ball bond (micron)	35	35	30	30	25	25	25	20	20
Pad pitch Wedge bond (micron)	30	25	25	25	20	20	20	20	20
Pad pitch Area array flip chip (micron)	150	130	130	130	120	120	120	110	110

2.2 Wire bonding techniques

Although flip chip has been widely adopted by high-end graphic, microprocessor chip, wire bonding is still popular in the cost-sensitive, low-level products which do not need many I/O connections.

Wire bonding uses a fine metal line which is usually made by gold or aluminum as the signal transmitting media. The technique simply applies heat, pressure, or ultrasonic vibration to weld the fine metal line onto the surface of metal pad. The wire bonding can divide into two types according to the bonding tool [9].

(1) Wedge Bonding [9, 11]

Based on the structural restriction of bonding tool, the direction of the fine line supplies should cooperate with wedge bonding tool, and the pad position and direction of loop should be the same with the direction of the fine line supplies as shown by Figure 2.1 (a). It is very inconvenience for operation because there is a need to adjust the direction between IC chip and substrate board.

(2) Ball Bonding [9, 11]

Ball bonding does not consider the direction of the fine line supplies, but it needs electronic flame off in the front of the metal during bonding process as shown in Figure 2.1 (b). It is convenience because it does not need to adjust the direction between IC chip and substrate board.

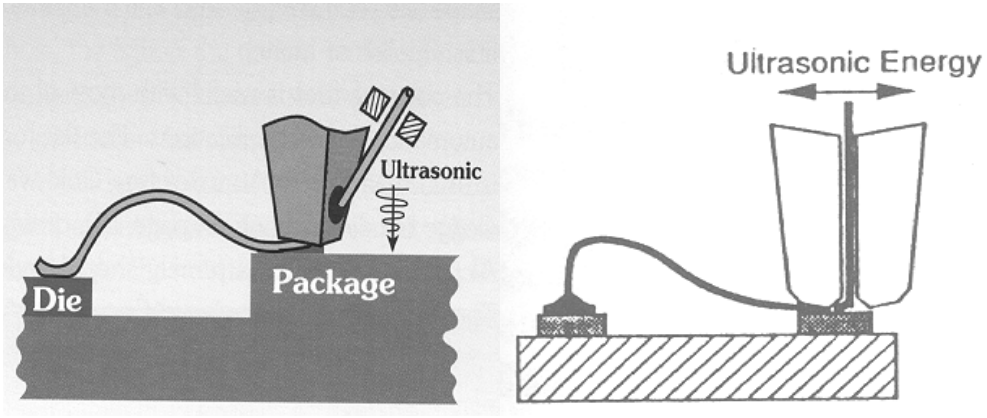

Figure 2.1 (a) Wedge bond (b) Ball bond

In addition, there are three types for the wire bonding based on its connective method [9, 11]:

1. Thermocompression

Thermocompression bonding requires a high-force on a surface with a high temperature, around 300 °C. It provides excellent, reliable Al-Au ball bonds. The wire material is gold (Au), but the pad materials can be Au or aluminum. The bonding mechanism is based on thermal diffusion.

2. Ultrasonic

Ultrasonic bonding uses Al bond wires under ambient temperature. Bonding is formed as a wedge bond by pressure and vibrational energy. The bonding mechanisms involve acoustic weakening, dynamic recovery, and recrystallization.

3. Thermosonic

Thermosonic bonding is used for Au wires and currently is accounting for about 90 % of all wire bonding. It is carried out at temperatures of around 150 °C to 250 °C. Bonding is formed when the ultrasonic energy combines with the capillary technique of thermocompression bonding. This method is better than thermocompression because of lower impact force and lower temperature which can reduce the intermetallic compounds formation during the bonding process.

According to the review of wire bonding above, the thermosonic, ball bond and gold wire are the major wire-bonding technologies as of today. Table 2.3 summarizes the operating temperature, wire materials, pad materials, and impact force among various wire bonding technologies. [9, 11]

Table 2.3 A comparison of three types of wire bonding technologies [9]

Wire bonding technology	Thermocompression	Ultrasonic	Thermosonic
Operating Temperature	300-500 °C	25 °C	100-240 °C
Wire Materials	Au	Au, Al	Au, Cu
Pad Materials	Al, Au	Al, Au	Al, Au
Impact force per wire	150~250mN	5~25mN	5~25mN
Note	High pressure, no ultrasonic energy	Low pressure with ultrasonic energy	Low pressure with ultrasonic energy

2.3 Current status of bond pad technology

Conventional bond pads are positioned on the outside of active circuits and uses bus to connect the active circuits as shown by Figure 2.2. According to Moore's law [1], the performance of IC device technology continues its advancement in speed as the minimum feature of transistor scales at 30 % every 18 months. As more functions and complexity are designed in the chips, which requires proportionally larger numbers of I/O connection. With the I/O numbers increasing, more areas are needed to accommodate active circuits. Nevertheless, the available area for active circuits becomes constraint if the conventional bond pad is used. Therefore, the size of conventional bond pad needs to be shrunk in order to have more areas for putting active circuits. However, the size of bond pad is limited by wire bonding process and technology. In order to relax the limitation of the areas of active circuits, a new method, BOAC (bonding pad over the active circuits) that puts the bond pad directly on the active circuits, has been developed as shown by Figure 2.3, 2.4 [2]. BOAC not only solves the confinement of the area but also shrinks the size of the chip. On-chip bussing and interconnect resistance are also reduced, because the bond pads could be located closer to the active circuit elements [3]. However, they may have mechanical problems such as debonding, delamination or failure during wire bonding if the mechanical support under pads is weak. Unfortunately, materials with weak mechanical properties such as porous low-k materials are needed to further reduce the RC delay in the backend interconnects. These weak, porous low-k materials will reduce the mechanical strength of BOAC structures and pose great concern in the mechanical reliability of BOAC design and structure. In the next section, we will discuss the RC delay and the need for low-k materials.

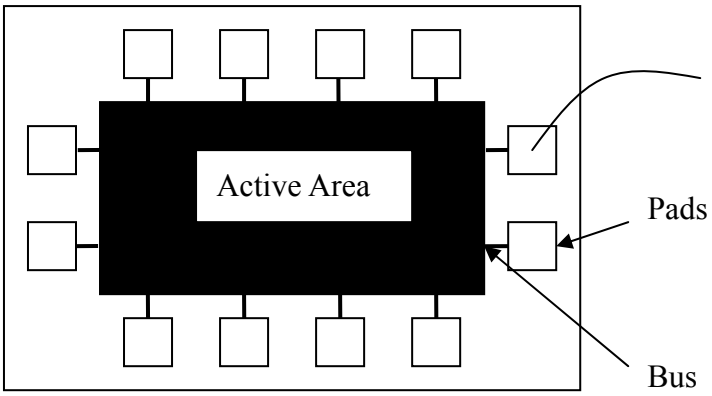

Figure 2.2 Top-view of Conventional Normal Pad

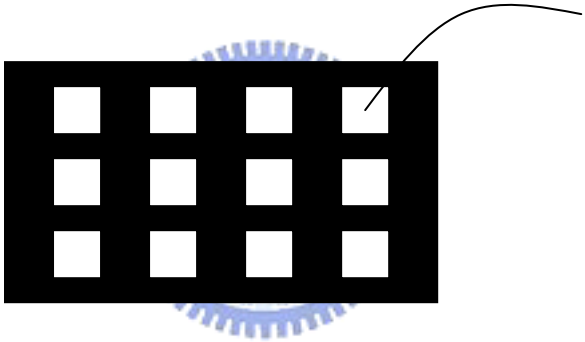

Figure 2.3 Top-view of BOAC (bonding pad over the active circuits)

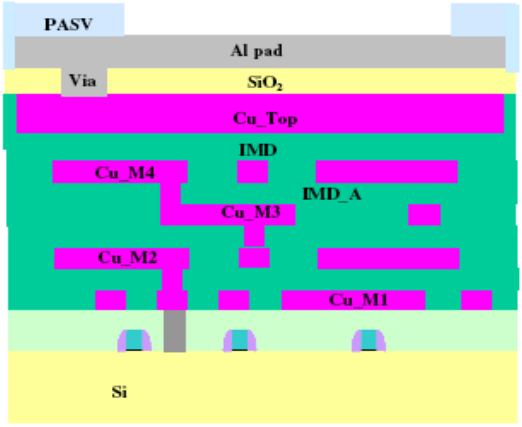

Figure 2.4 Cross-section of BOAC [2]

2.4 Evolution of IC interconnect technology

Aluminum line and SiO_2 are the main materials used in the backend interconnect since the dawn of IC industry. However, when IC technology node scales down to 0.25 μm and below, the wire signal delay in backend interconnect has become the bottleneck in the RC delay as shown by Figure 2.5 [12]. The equation for RC delay can be expressed by Equation 2.1.

$$RC = 2 \times \rho \times \kappa \times \varepsilon_0 \left(\frac{4L^2}{P^2} \times \frac{L^2}{T^2}\right) \quad (2.1)\ [13]$$

Where ρ is resistivity of metal line, κ is dielectric constant of ILD and L, T, P are the length, thickness, and width of the metal line. Therefore, P will reduce and L will increase according to the Moore's law [1]. In order to reduce the RC delay, there are two main approaches. One is to reduce the resistivity of metal line by replacing Al wire with copper and the other is to reduce dielectric constant of ILD material by replacing SiO_2 with low-k materials.

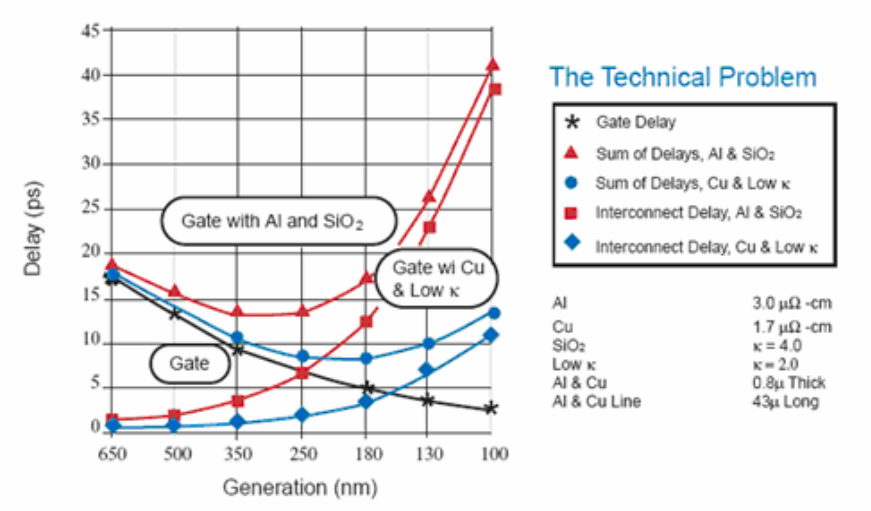

Figure 2.5 Interconnect ε, Gate Delay versus technology node [12]

2.4.1 Development of Copper Interconnects

In September 1997, IBM first announced copper damascene process for the microprocessor products [14]. The advantages of copper are low resistivity (Cu: 1.67 μΩ-cm, Al: 2.66 μΩ-cm), high resistance of the electron migration, and high reliability [15]. Besides, new copper technology lowers the cost of process by using damascene process which utilizes dual damascene process to reduce process step.

2.4.2 Development of Low-k materials

In order to reduce the RC delay, the ILD choice is to change from SiO_2 (k=3.9~4.2) to low-k materials for the reduction of to the capacitance. Therefore the basic requirements of low-k materials are (1) low dielectric constant, (2) high insulation, (3) high mechanical strength, (4) high heat conduction, (5) high heat stability and (6) low moisture uptake etc [15-16]

In 2006 ITRS report as shown in Table 2.4 [10], the dielectric constant will be reduced to 2.0 in 2013. Although there are many ways to reduce the dielectric constant with many low-k materials options, there are many challenges to achieve a dielectric constant below 2.5 [15-18], which is categorized as ultra low-k in the industry. Currently, the porous materials are favored the most because its dielectric constant can reach easily below 2.5 [19]. But, the ultra low-k porous materials do not possess good mechanical strength because of its loose structures and may incur problems such as fracture, delamination and failure during IC processing. Specifically, the elastic modulus of ultra-low-k is only 1/10 times to that of conventional SiO_2 (72GPa) [4-5] while its thermal stress is usually small tensile stress [20]. Low modulus and tensile stress imply that low mechanical strength and low resistance of fracture. In summary, the mechanical integrity and reliability of porous low-k

materials is worse than that of conventional SiO_2 when experiencing subjecting to external forces such as CMP, wire bonding, probing and wafer test etc. in the chip making process.

The mechanical properties of ultra-low-k materials also include the adhesion to the neighbor materials. Ultra-low-k materials have lower adhesion due to porosity and the mismatch of CTE may damage the interface during the manufacture process or component operation **[21]**. When these ultra-low-k materials are used in the devices, the devices are easily over the yield strength under the external forces, which may increases the probability of devices failure.

Table 2.4 2006 ITRS report : Road map of dielectric constant [10]

	2005	2006	2007	2008	2009	2010
Interlevel metal insulator-effective dielectric constant (κ)	3.1~3.4	3.1~3.4	2.7~3.0	2.7~3.0	2.5~2.8	2.5~2.8
Interlevel metal insulator-bulk dielectric constant (κ) (was)	≦ 2.7	≦ 2.7	≦ 2.4	≦ 2.4	≦ 2.2	≦ 2.2
Interlevel metal insulator-bulk dielectric constant (κ) (is)	2.6~3.0	2.6~3.0	2.3~2.7	2.3~2.7	2.1~2.4	2.1~2.4
	2011	2012	2013			
Interlevel metal insulator-effective dielectric constant (κ)	2.5~2.8	2.1~2.4	2.1~2.4			
Interlevel metal insulator-bulk dielectric constant (κ) (was)	≦ 2.2	≦ 2.0	≦ 2.0			
Interlevel metal insulator-bulk dielectric constant (κ) (is)	2.1~2.4	1.8~2.1	1.8~2.1			

2.5 The challenges in bond pad design

In the previous sections, current devices process and technology involves the copper line, low-k materials for ILD and bond pad over active circuit instead of conventional normal pad without active circuit under it. The mechanical weakness of these low-k materials may induce reliability problems such as delamination and cracks or devices failure. In the conventional process, pad structure has no active circuits underneath and uses SiO_2 as the interlayer dielectric (ILD) material. It possesses strong mechanical strength which can resist the impact force from wire bonding or wafer probe.

Nowadays the active circuits have been implemented under the bond pad and the ILD has changed from SiO_2 to porous low-k materials. The elastic moduli of low-k materials are 7-10 times lower than that of SiO_2 [4-5]. In addition, the adhesion of porous low-k dielectric is poor. It decreases with decreasing dielectric constant [22]. Therefore, ultra-low-k maetrials will weaken the mechanical strength of BOAC structures. The devices with poor mechanical strength may fail due to the impact force from wire bonding or wafer test. Heinen *et al.* proposed a BOAC scheme by implementing an additional metal layer with via connecting to the active circuits beneath the bond pad and adding a polyimide as a stress buffer layer between the inorganic cover coat and top metal layer [2]. Chou *et al.* used a thick aluminum film (at least 1.2 μm), which formed on the top copper metal film, and served as a very effective buffer layer against bonding stress [23]. Both focused on the incorporation of stress absorbing or dissipating layer below the bond pad to mitigate the force applied to the pad during wire bonding. A recent paper by Hess *et al.* approached BOAC using a new layout technology without above-mentioned stress buffer layer [24]. Wire bonding assembly and package stress reliability were evaluated for two

BOAC layouts in conjunction with mechanical simulation. The reliability result between the two different BOAC layouts was partially explained through a simplified mechanical simulation of the pad structures during wire bonding. To analyze the mechanisms of the mechanical strength of BOAC structures, B. Chandran simulated the mechanical stress induced in the die back-end layers due to the package, and also identified the key parameters that impact these stresses [25]. In addition, modeling [6-7] has been employed to understand the stress impact to the wire bonding process and BOAC. D. Degryse simulated the deformation and stress during different forces of wire bonding and found that the Poisson ratio of the dielectric layer is an important parameter to control the stress except the stiffness of low-k materials [26]. In order to know the mechanical problems of low-k material, S. Allada discussed the issues of low-k adhesion on BOAC structures that low adhesion would easily induced the delamination [21]. Several researchers even used area release rate to analyze the damage sensitivity [21, 27]. These studies had only one objective; that is to design a perfect BOAC structures which can resist the impact force form wire bonding when the ultra low-k materials are used as the ILD

2.6 Motivation of Thesis

From previous sections, we realized that although BOAC can relax the constraints on bond pad size and pitch and may reduce the die size, BOAC with poor mechanical strength may suffer mechanical damage such as delamination, cracks or devices failure during fabrication, probing and wire bonding processes. However, it is too complicate to test every BOAC design. In addition, there is no such a standard for differentiating which BOAC structures can pass the mechanical damage. Therefore a methodology for quick screening various BOAC design is highly desirable in the low-k/Cu interconnects under demanding technology development cycle environment.

It has been well known that nanoindentation is one of the important technologies to measure the mechanical properties of thin films. Nanoindentation used load–displacement relation to evaluate the mechanical properties of thin films, such as hardness and modulus. In the pass few decades, many researchers worked on thin films properties using nanoindentation with different materials, different thicknesses and different substrates. Hertz built the contact deformation and mechanics to provide the basic theory for nanoindentation [28]. Seddon (1965) [29] derived the relation between the indenter, loading, displacement and the contact area. The results showed that the relation of loading-displacement can be expressed in exponent law ($p = \alpha h^m$) for easy-shape indenter. Oliver and Pharr (1989) [30] derived an equation to evaluate non-linear loading and developed a method to evaluate the modulus. Oliver and Pharr (1992) [31] discovered that the loading-displacement curves were all non-linear and they developed the continuous stiffness measurement (CSM) to evaluate the modulus. Furthermore, A. A. Volinsky [32] used nanoindentation to measure the fracture toughness, adhesion and mechanical properties of low-k dielectric thin films.

Nonetheless, we wondered if the nanoindentation can evaluate the mechanical strength of BOAC structures since nanoindentation was usually used to measure the thin film's mechanical properties. Bhattacharya and Nix (1988) [33] found the relation between indenter depth and thickness of thin film, the modulus was affected by the substrate's modulus with the indenter depth increasing. And King (1987) [34] derived the relation between the indenter geometry and the ratio of the parameters related to indenter depth. It indicated that the thin film's modulus would be affected by the substrate's modulus when using nanoindentation. Therefore, nanoindentation, which simulates the impact force of wire bonding, is chosen in this thesis to analyze the mechanical strength of BOAC structures by exploring the substrate effect in a multi-layered copper/low-k interconnects.

The purposes of this study are (1) to establish a quick turn-around methodology for different BOAC structures, (2) to quantify the mechanical strength of BOAC structures, (3) to establish a success criteria of minimum required mechanical strength without bondability fails, and (4) to build a model that can predict the mechanical strength of BOAC structures from nanoindentation measurements and discuss the model's applicability and problems.

Two different BOAC stacks were investigated in this thesis. The first BOAC structure was Al/composite substrate system which could be categorized as a soft film/hard substrate system. The other BOAC structure was oxide/composite substrate system which could be categorized as a hard film/soft substrate system. The objective is to cross-check the fitting results and to understand any difference of the values obtained from nanoindentation method.

Chapter 3 Experimental Methods

3.1 Sample Preparation

3.1.1 BOAC and Normal pad samples

First, we used one specific normal pad and BOAC pad to introduce their design and difference as shown by Figures 3.1 (a) and (b). Normal pad had full array of dummified trench/via under the bond pad and without active devices. BOAC had little trench/via and with active devices under the bond pad. Also, BOAC needed some buffer layer such as fluorinated silicate glass (FSG) to protect the active devices under the bond pad. In this thesis, we would investigate the mechanical strength of the structures under the BOAC pad using several different BOAC samples with different designs.

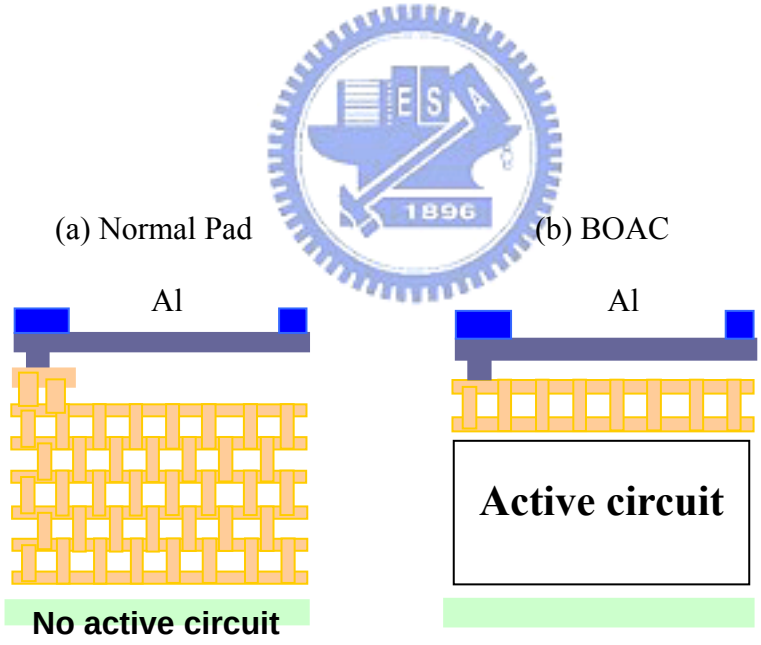

Figure 3.1 Cross-sectional view of (a) Normal Pad (b) BOAC

There were 7 different BOAC structures in our study. The differences of these structures were listed below:

1. Different technology nodes (90 nm *vs.* 65 nm)
2. Different low-k materials (low-k *vs.* ultra low-k)
3. Different bond pad structures (BOAC *vs.* conventional Normal pad)
4. Different copper density (Top metal: metal block *vs.* metal ring)

We used these 4 different parameters to analyze the mechanical strength of BOAC structures and to see if we can distinguish the stronger one from the weaker one. The samples were prepared by UMC using 90 nm (7 metal layers) and 65 nm (6 metal layers) copper damascene technology. The cross-sectional diagrams of these BOAC typically included Al pad, oxide, FSG/copper M7 or M6 layer as the top metal layer depending on the 65 or 90 nm technology node, low-k materials with active circuits in M1-6 or M1-5, oxide, Si from top to the bottom as illustrated by Figures 3.2 and 3.3. The cross-sectional diagram of conventional Normal Pad included Al pad, oxide, FSG/copper M7 or M6 layers, low-k materials with a full array of dummified trench/via reinforcement in M1-6 or M1-5, oxide, Si from top to the bottom as illustrated by Figure 3.4. The details of these 7 BOAC structures were listed in Table 3.1. Moreover, we separated these 7 BOAC structures into 4 groups and each group had only one different parameter as shown in Table 3.2. The purpose was to analyze the effect of each parameter.

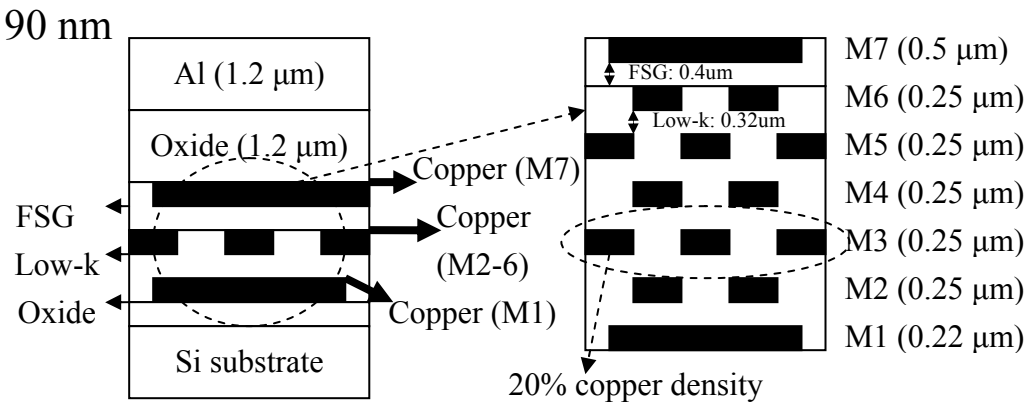

Figure 3.2 The cross-sectional view of BOAC in 90 nm process

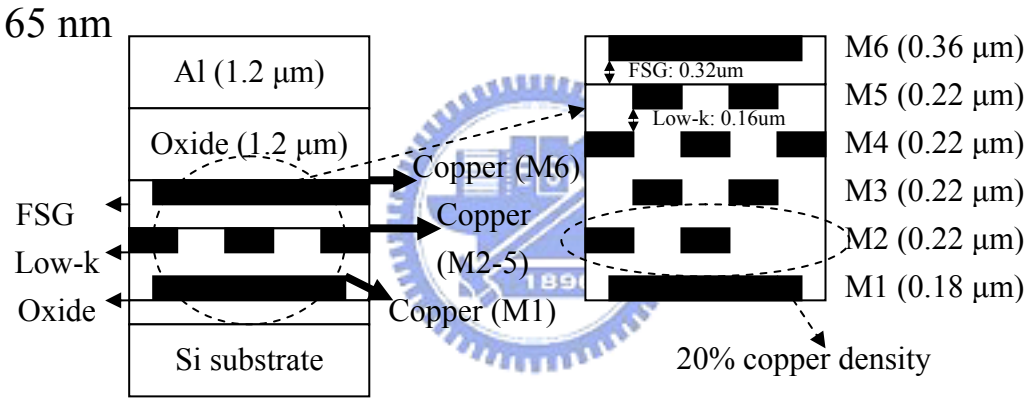

Figure 3.3 The cross-sectional view of BOAC in 65 nm process

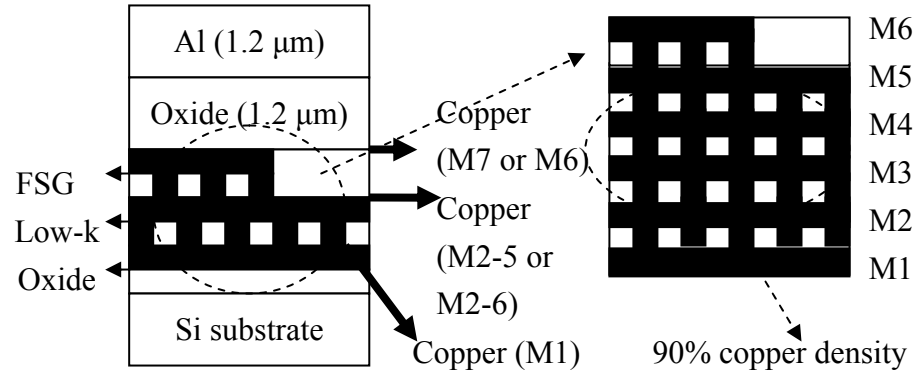

Figure 3.4 The cross-sectional view of Normal Pad

Table 3.1 The details of BOAC structures used in this study

Code name for BOAC samples	Technology nodes	Copper Density (TopM7 orM6)	Copper Density (M1-6 orM1-7)	Low-k materials	Pad types
1.90LKBOAC A	90 nm	Block (90 %)	20 %	LK	BOAC
2.90LKBOAC B	90 nm	Ring (20 %)	20 %	LK	BOAC
3.90LKNormal	90 nm	Block (90 %)	90 %	LK	Normal
4.65LKBOAC	65 nm	Block (90 %)	20 %	LK	BOAC
5.65LKNormal	65 nm	Block (90 %)	90 %	LK	Normal
6.65ULKBOAC	65 nm	Block (90 %)	20 %	ULK	BOAC
7.65ULKNormal	65 nm	Block (90 %)	90 %	ULK	Normal

Table 3.2 4 parameters of BOAC structures under study

Group	Parameter	Samples
1	Bond pad	90LKBOAC **A** *vs*. 90LK**Normal**
2	Copper density (top layer)	90LKBOAC **A** *vs.* 90LKBOAC **B**
3	Technology nodes	**90**LKBOAC A *vs.* **65**LKBOAC
4	Low-k materials	65**LK**BOAC *vs.* 65**ULK**BOAC

3.1.2 Blank films

In order to analyze the mechanical strength of various BOAC structures accurately, the mechanical properties of specific films in the BOAC structure will be measured. Five blank films listed in Table 3.3 were deposited onto 8-inch silicon wafer by UMC. These wafers were cut into 10 mm x 10 mm square for specific measurement. The mechanical properties of these materials were measured by nanoindentation.

Table 3.3 Materials and thickness of blanket films used in the BOAC stack

Material	Thickness (nm)
Al (Aluminum)	2000
Cu (Copper)	1000
FSG (Fluorinated Silica Glass)	1000
PEOX (Oxide)	1000
Low-k (Novellus Coral™)	1000

3.2 Experimental method and procedure

3.2.1 Nanoindentation Measurement of Blank Films

Nanoindentation was employed to characterize the basic mechanical properties of blank films such as Al, Cu, FSG, PEOX (Oxide) and low-k. 10 indentation tests were taken to ensure reproducibility and the average of these indentations was reported in this study. The indentation depth was up to 1.0 μm for these blank films. For the data collection, we choose the average value at one-tenth (1/10) of the film thickness to avoid the substrate effect.

3.2.2 Nanoindentation Measurement of BOAC structures

Next nanoindentation was used to characterize the mechanical properties of various BOAC structures. The indentation depth was up to 2.0 μm for the tip traveling through Al pad (1.2 μm thick) into oxide layer. For each BOAC structure, 5 indentation tests were taken to ensure reproducibility and the average of these indentations was reported. For each indentation mark, which should be placed in the center of the pad (the pad we choose here were 40 μm x 40 μm), scanning electron microscope (SEM) was used to check the indentation marks to ensure correct measurement and data analysis. Our approach is to take advantage of the substrate effect in the nanoindentation to distinguish the mechanical strength of the BOAC structures (multi-layered metal/dielectric interconnects) beneath Al pads from the raw data ($E_f^{\text{nanoindentation}}$). We assumed that the structure under the Al pad as a uniform layer and built a two-layered model (Al/composite substrate) to quantify the modulus of composite substrate (E_{cs}) using curve fitting. The data analysis will be described in detail in the following section entitled “Introduction of Instruments”.

Overall, this thesis will investigate the effects of metal density, dielectric materials,

technology node, and pad design on the rigidity of BOAC structures and its correlation with bondability test. Furthermore, the applicability and issues of this methodology for predicting the mechanical strength of BOAC structures will be also discussed and addressed.

In the first stage, nanoindentation will apply directly onto Al pads of BOAC structures *i.e.* an Al/composite substrate system which can be categorized as a soft film/hard substrate system. The result obtained by fitting method will be cross-checked by applying nanoindentation onto oxide/composite substrate system after removing Al pad material, which can be categorized as a hard film/soft substrate system.

3.2.3 Etch process for the removal of Al pads

For preparing hard film/soft substrate system, we etched off Al pad from original BOAC samples. BOAC samples were dipped into an aluminum etch solution which was composed of phosphoric acid, acetic acid, nitric acid, kept at 55 ℃, for 5 minutes. Water rinsing and drying of samples were followed as shown by Figure 3.5.

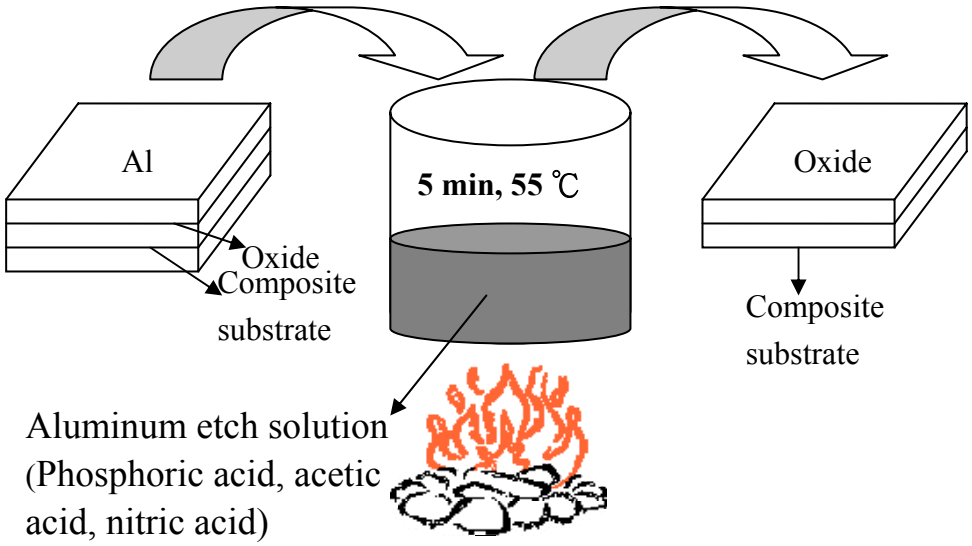

Figure 3.5 Al pad etching process

Experimental procedures:

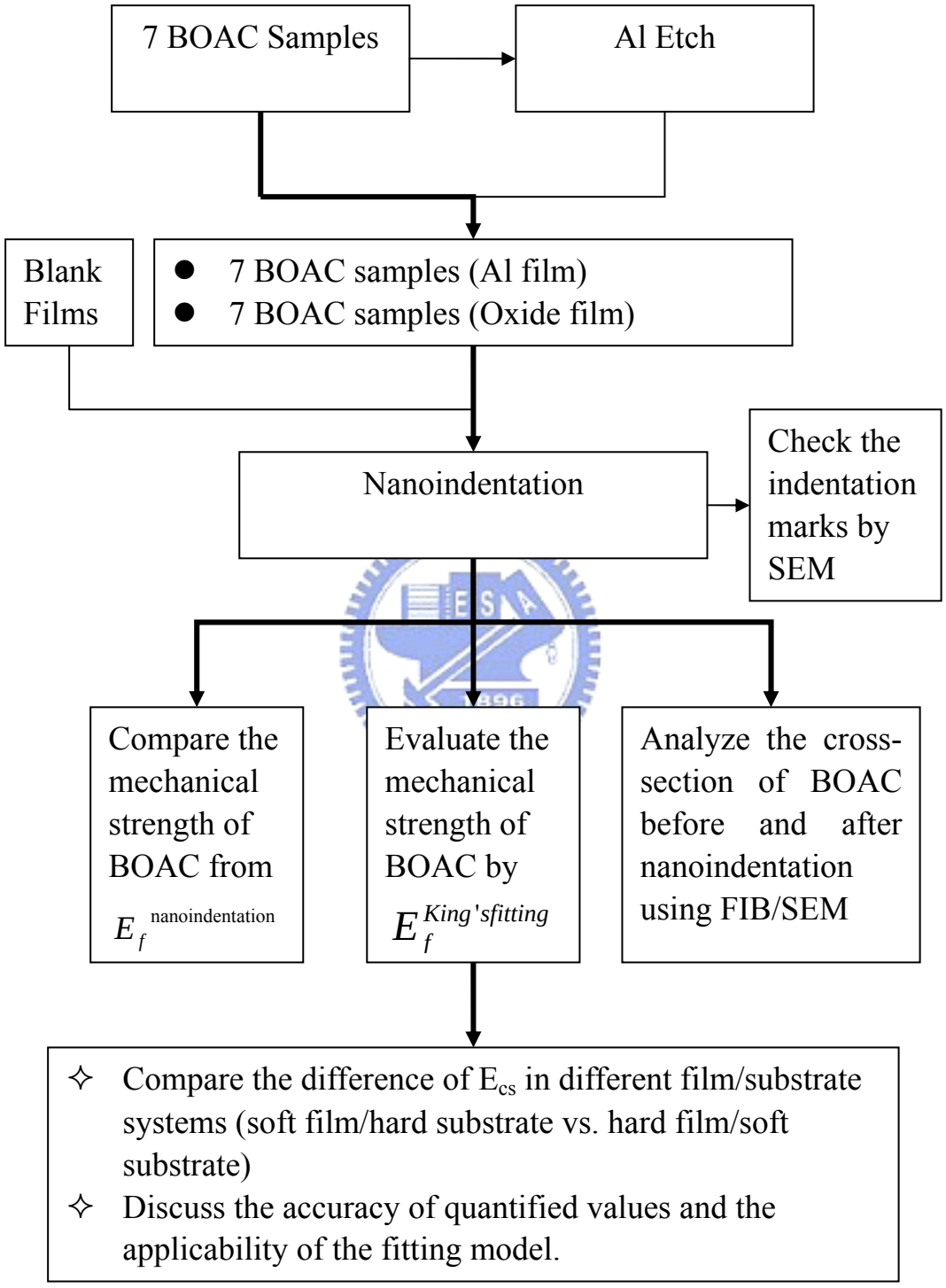

Figure 3.6 Flow-chart of experimental procedures

3.3 Introduction of Instruments

3.3.1 Nanoindentation

Nanoindentation has been commonly used for measuring modulus and hardness. In this study, nanoindentation system used was a MTS, Nano Indenter XP system with a Berkovich tip in a continuous stiffness mode (CSM) at a constant strain rate 0.05 s^{-1} as shown by Figure 3.7. Nanoindentation used load–displacement relation illustrated by Figure 3.8 to characterize the mechanical properties of thin films. We evaluated the contact area in maximum loading during unloading process. The hardness was defined as the average pressure during loading [35]:

$$H = \frac{P_{\max}}{A} \tag{3.1}$$

H: hardness

P_{max}: maximum loading

A: projected area of elastic contact

($A=24.5h_c^2+C_1h_c^1+C_2h_c^{1/2}+C_3h_c^{1/4}+\ldots\ldots \fallingdotseq 24.5h_c^2$)

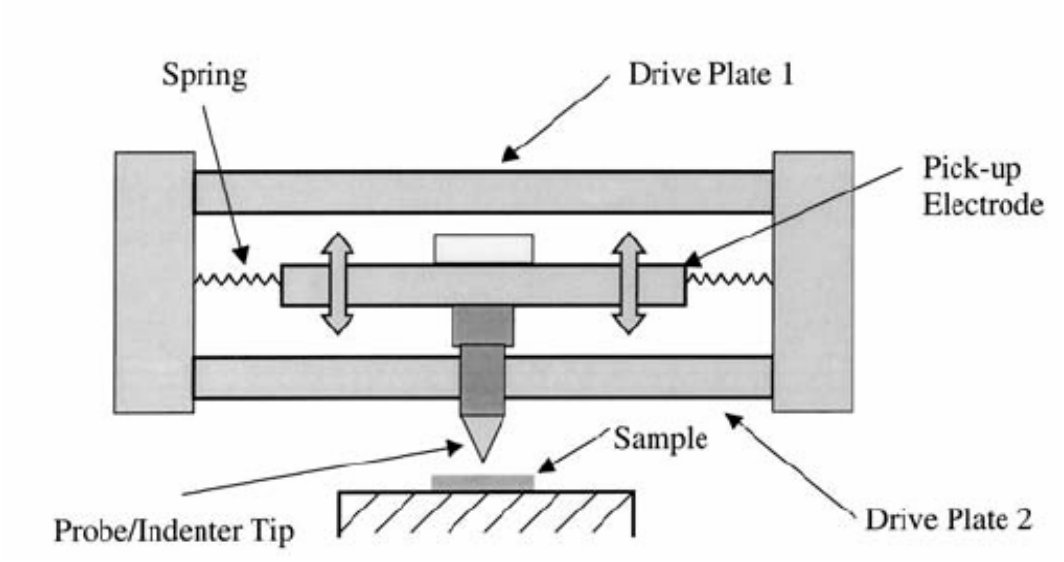

Figure 3.7 Schematic diagram of a nanoindentation system

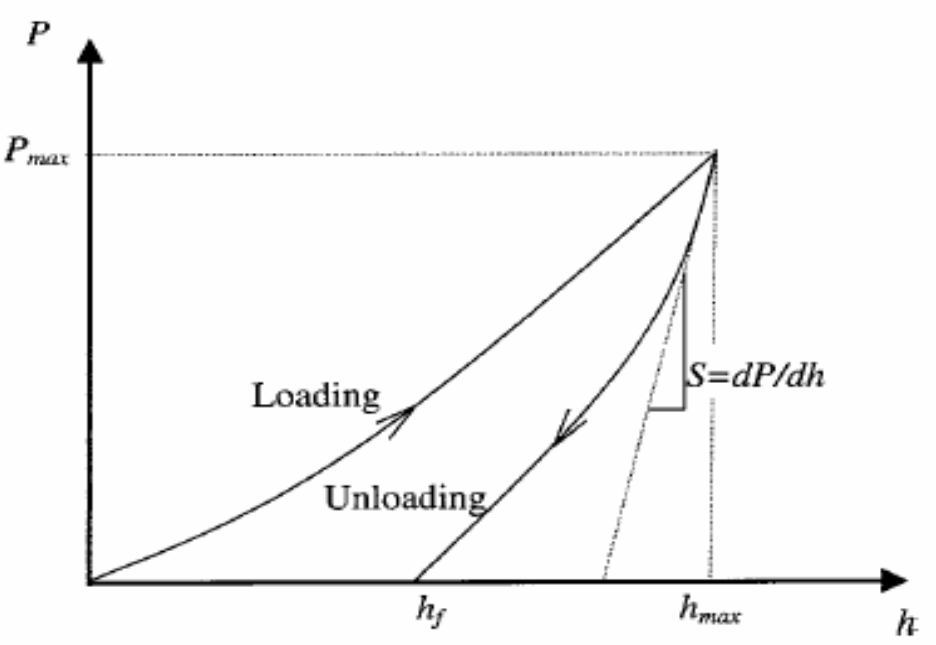

Figure 3.8 Load-Displacement of Nanoindentation

For a single film structure, Oliver and Pharr analysis method [31] was employed for nanoindentation measurement. The reduced Young's modulus, E_r can be obtained by Equation (3.2):

$$E_r = \frac{\sqrt{\pi}}{2\beta}\frac{S}{\sqrt{A}} = \frac{\sqrt{\pi}}{2\beta}\frac{1}{\sqrt{A}}\frac{dP}{dh} \tag{3.2}$$

where

E_r: reduced modulus

ß: constant depending on the geometry of the indenter

A: projected area of elastic contact

$S = \frac{dP}{dh}$: the slope of the load–displacement curve at the beginning of the unloading stage as illustrated in Figure 3.8

E_r can be further expressed in terms of modulus and poisson's ratio of film and indenter by Equation (3.3):

$$\frac{1}{E_r} = \frac{(1-\nu_f{}^2)}{E_f} + \frac{(1-\nu_i{}^2)}{E_i} \tag{3.3}$$

where

E_i, ν_i: Modulus and Poisson's ratio of the indenter

E_f, ν_f: Modulus and Poisson's ratio of the specimen

Combining Equation (3.2) and Equation (3.3), the modulus of thin film, E_f is rearranged as a function of penetration depth in our measurement and expressed by Equation (3.4).

$$E_f = \frac{(1-\nu_f^2)}{\frac{1}{E_r} - \frac{(1-\nu_i^2)}{E_i}} \tag{3.4}$$

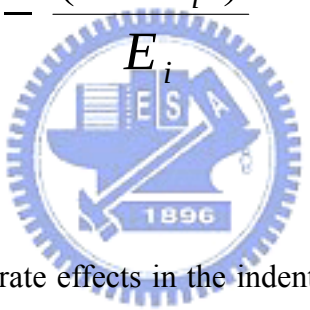

3.3.1.1 Substrate Effects

In this study, we used substrate effects in the indentation measurement to quantify and compare the mechanical strength of various BOAC structures underneath Al pad. Prior research found that the film's mechanical properties (modulus, hardness) were affected by the substrate in nanoindentation test for either soft film on hard substrate [33-34] or hard film on soft substrate [33-34]. Although the substrate effects were deemed as a drawback and complication in the extraction of modulus and hardness data, we specifically utilize this substrate effect to analyze the mechanical strength of the substrate underneath Al pad. King's equation [34] dealt with the substrate effect in the indentation and related E_r with substrate's modulus as expressed by Equation 3.5:

$$\frac{1}{E_r} = \frac{(1-\nu_i^2)}{E_i} + \frac{(1-\nu_f{}^2)}{E_f}(1-e^{-\alpha\frac{t}{a}}) + \frac{(1-\nu_s^2)}{Es}e^{-\alpha\frac{t}{a}} \quad (3.5)$$

where

E_r: reduced modulus

E_i, ν_i : Modulus and Poisson's ratio of the indenter

E_f, ν_f : Modulus and Poisson's ratio of the film

E_s, ν_s : Modulus and Poisson's ratio of the substrate

α : Constant related to the indenter geometry

a: 4.95h and h: Indenter depth

t: Film thickness under the indenter

In our study, assuming that E_i, ν_i ,E_f and ν_f were constants, and $\nu_i=\nu_f=\nu_s$, Equation 3.5 can be further simplified into Equation 3.6:

$$\frac{1}{E_r} = A + B + C \times e^{-\alpha\frac{t}{a}}\left(\frac{E_f - E_s}{E_s \times E_f}\right) \quad (3.6)$$

Where A, B and C were constants, and $e^{-\alpha\frac{t}{a}}$ would increase with increasing indenter depth.

$\frac{1}{E_r}$ would change as a function of $\left(\frac{E_f - E_s}{E_s \times E_f}\right)$ in three cases listed below and illustrated by Figure 3.9:

Case 1: $E_s = E_f$. The modulus of film was the same as that of the substrate.

E_r remained constant.

Case 2: $E_s > E_f$. The modulus of film was larger than that of the substrate.

$\frac{1}{E_r}$ decreased with increasing indenter depth. Therefore, E_r would increase with increasing indenter depth. $\frac{1}{E_r}$ decreased with increasing E_s. Therefore, E_r would increase with increasing E_s.

Case 3: $E_s < E_f$. The modulus of film was smaller than that of the substrate.

$\frac{1}{E_r}$ increased with increasing indenter depth. Therefore, E_r would decrease with increasing indenter depth. $\frac{1}{E_r}$ increased with increasing E_s. Therefore, E_r would decrease with increasing E_s.

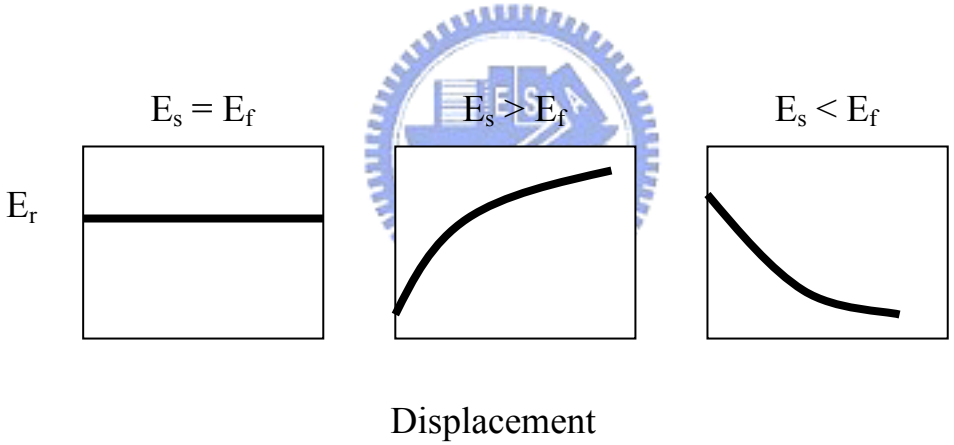

Figure 3.9 The relationship of E_r and E_s, E_f as a function of displacement

The experimental data $E_f^{\text{nanoindentation}}$ was measured from E_r using Oliver–Pharr method by Equation 3.3. If ν_f , ν_i , E_i were constants, $E_f^{\text{nanoindentation}}$ was directly proportional to E_r. As a result, we can easily compare the mechanical strength of BOAC structures from $E_f^{\text{nanoindentation}}$ as a function of displacement.

3.3.1.2 King's model Fitting

In order to evaluate the mechanical strength of BOAC structures, King's model was used to fit the experimental data from nanoindentation in order to evaluate E_s from Equation 3.4:

$$E_f^{\text{nanoindentation}} = \frac{(1-\nu_f^2)}{\frac{1}{E_r} - \frac{(1-\nu_i^2)}{E_i}} \tag{3.4}$$

Then, rearranging King's equation (Equation 3.5) into Equation 3.7 whose left-side equaled to the right-side of Equation 3.4.

$$\frac{(1-\nu_f{}^2)}{\frac{1}{E_r} - \frac{(1-\nu_i^2)}{E_i}} = \frac{(1-\nu_f{}^2)}{\frac{(1-\nu_f{}^2)}{E_f}(1-e^{-\alpha\frac{t}{a}}) + \frac{(1-\nu_s^2)}{Es}e^{-\alpha\frac{t}{a}}} \tag{3.7}$$

Moreover, Equation 3.7 can be defined as $E_f^{King'sfitting}$ as described by Equation 3.8:

$$E_f^{King's-fitting} = \frac{(1-\nu_f{}^2)}{\frac{(1-\nu_f{}^2)}{E_f}(1-e^{-\alpha\frac{t}{a}}) + \frac{(1-\nu_s^2)}{Es}e^{-\alpha\frac{t}{a}}} \tag{3.8}$$

Finally, using $E_f^{King'sfitting}$ to fit raw data from $E_f^{\text{nanoindentation}}$, and evaluate the mechanical strength of various BOAC structure through the extraction of E_s. Here the BOAC structure was treated as a two-layered model as schematically illustrated by Figure 3.10(a) for Al/composite BOAC substrate and Figure 3.10(b) for

oxide/composite BOAC substrate after removing Al layer. The composite BOAC substrate was assumed as one uniform layer. Before the fitting, we needed to confirm some of parameters in the Equation 3.8:

$v_f = v_s = 0.25$

a=4.95h, h=Indenter depth

t= Film thickness under the indenter. The film (Al or Oxide) thickness was 1200 nm. Therefore, t + h=1200 as shown in Figure 3.10(c).

α =Constant related to the indenter geometry. Here we use the data from King's and Nix's papers as shown in Figure 3.11 **[34, 36]**.

E_f of Al or Oxide film was obtained from our own measurement of blanket film as summarize in Chapter 4.1.

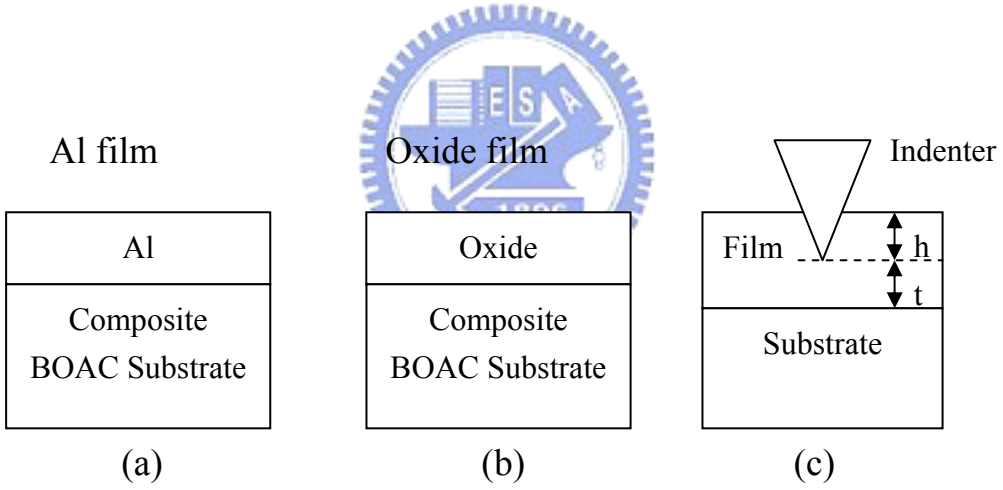

Figure 3.10 (a) two-layered model of Al system (b) two-layered model of oxide system (c) two-layered model : the relationship between h and t

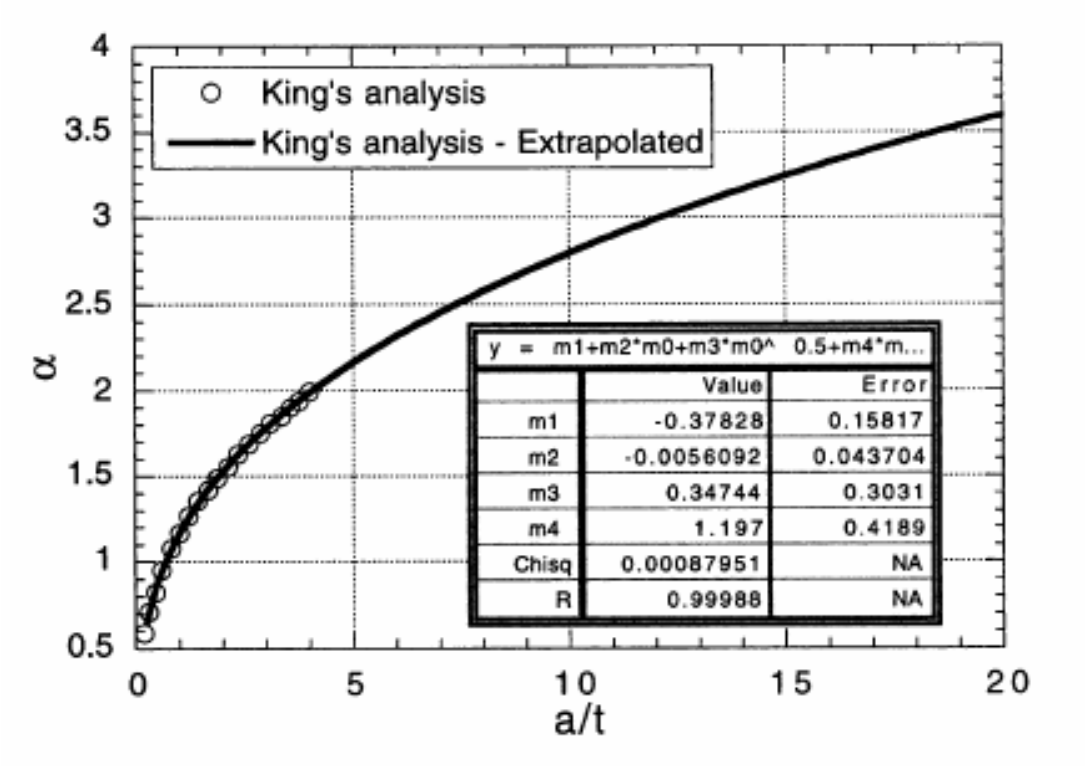

Figure 3.11 α **vs. a/t [36]**

3.3.2 Focus Ion Beam (FIB)

Similar to SEM, the ion beam of FIB is generated in a liquid-metal ion source (LMIS) instead of an electron beam. Most FIB system used a gallium ion (Ga^{+}) beam because of low melting point, low vapor pressure and good resistant of oxidization. In this study, Dual Beam (focused ion beam and electron beam) system located in NCTU was used to cut the cross-section of BOAC structures and analyze the relationship between the fracture and the design of BOAC structures before and after indentation test.

Chapter 4 Results and Discussion

4.1 Measurement Results

4.1.1 Nanoindentation results of blank films

Table 4.1 showed the mechanical properties of materials commonly used in the multi-layered, patterned BOAC structures as illustrated in Figures 3.2 through 3.4. All blanket films except ultra low-k were measured by nanoindentation at NCTU. The data for ultra low-k were kindly provided by UMC. These basic properties would be used for quantitative analysis and discussion in the later chapter.

Table 4.1 The modulus and hardness of blank films in BOAC structures

Materials	Modulus (GPa)	Std. Dev. (GPa)	Hardness (GPa)	Std. Dev. (GPa)
Al	69.2	3.0	0.25	0.03
Cu	137.2	6.1	1.31	0.19
FSG	64.0	2.8	6.68	0.45
Low-k	15.4	1.0	2.24	0.17
oxide	79.5	3.4	7.80	0.53
Si	182.8	3.2	12.56	0.39
Ultra low-k	9	n/a	n/a	n/a

4.1.2 BOAC structures

4.1.2.1 Identification of indentations' positions

To ensure the accuracy of the measurement, indentation marks, which should be placed in the center of the pad, were verified by SEM. Figure 4.1 showed SEM top-view graph of 90nm BOAC parts after indentation test, indicating that indentation marks were truly placed in the center of the pad. The same procedure was employed for the other BOAC samples to ensure proper indentation tests with correct marking.

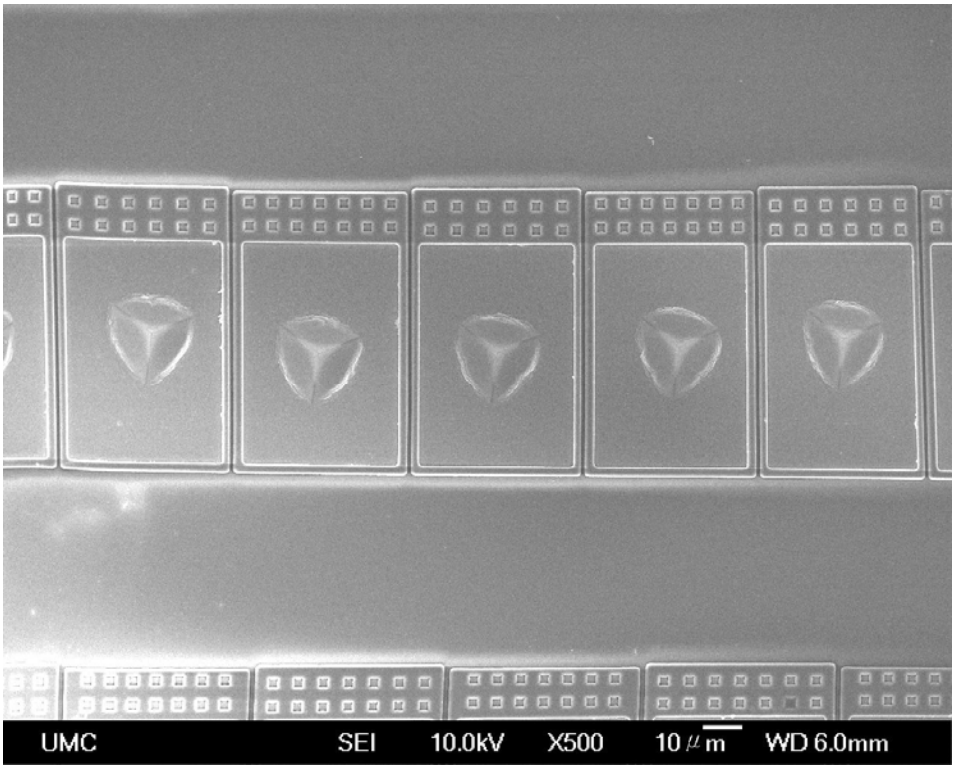

Figure 4.1 SEM top-view graph of indentation makes and their locations

4.1.2.2 Nanoindentation results of BOAC structures

First we took 2 BOAC structures fabricated for 90 nm technology (90LKBOAC A and 90LKNormal) as an example to demonstrate how we use nanoindentation to quantify the mechanical strength of BOAC structures. These 2 structures had the same Al pad, but different substrate structures under Al pad, whose cross-sectional diagrams have been shown in Figure 3.2 and 3.4. The 90LKNormal had full array of dummified trench/via in Cu/ILD. Therefore, the 90LKBOAC A only had sparse via in Cu/ILD. Figure 4.2 showed the nanoindentation results of these 2 BOAC structures.

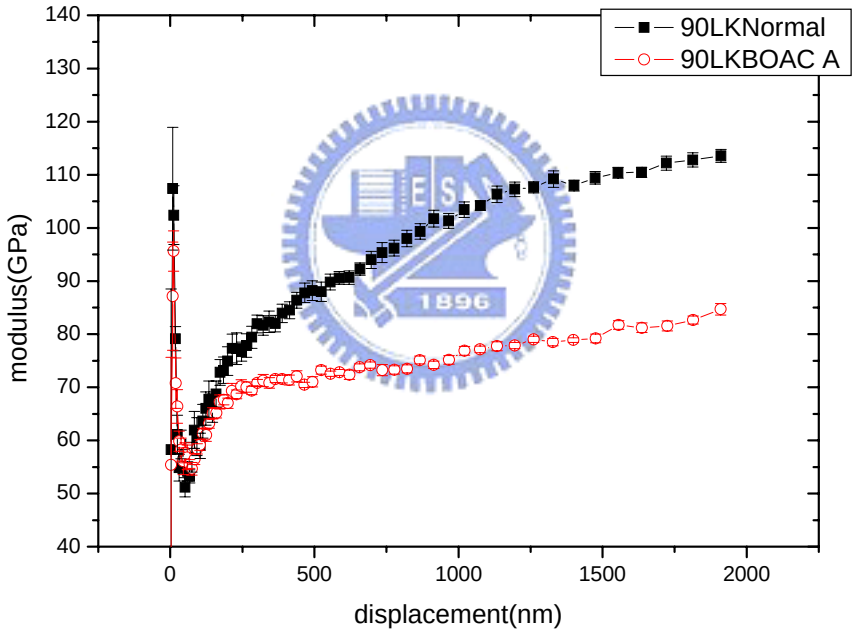

Figure 4.2 Nanoindentation results of 90LKBOAC A and 90LKNormal

In chapter 3, we had already explained how to distinguish the different substrate effects for a given film/substrate system. $E_f^{\text{nanoindentation}}$ would increase with increasing indenter depth and E_s when the E_s (modulus of substrate) was larger than E_f (modulus of film). From Figure 4.2, the modulus ($E_f^{\text{nanoindentation}}$) of 90LKNormal was

obviously larger than that of 90LKBOAC A, indicating that the modulus of composite substrate E_{cs} of 90LKNormal was stronger than that of 90LKBOAC A.

This method was also used for all BOAC structures. Figure 4.3 showed the nanoindentation results of all BOAC structures. The mechanical strength of all BOAC substrates E_{cs} in decreasing order was 65LKNormal > 65ULKNormal > 90LKNormal > 65LKBOAC > 90LKBOACA > 65ULKBOAC > 90LKBOACB.

Based on these results, we can establish that nanoindentation test was easy and quick to compare the mechanical strength of various BOAC structures underneath Al pad. Therefore, this thesis intends to set up a methodology to differentiate if the BOAC structures can pass the wire bonding or wafer testing by quantitative analysis of the mechanical strength of BOAC structures in the next section.

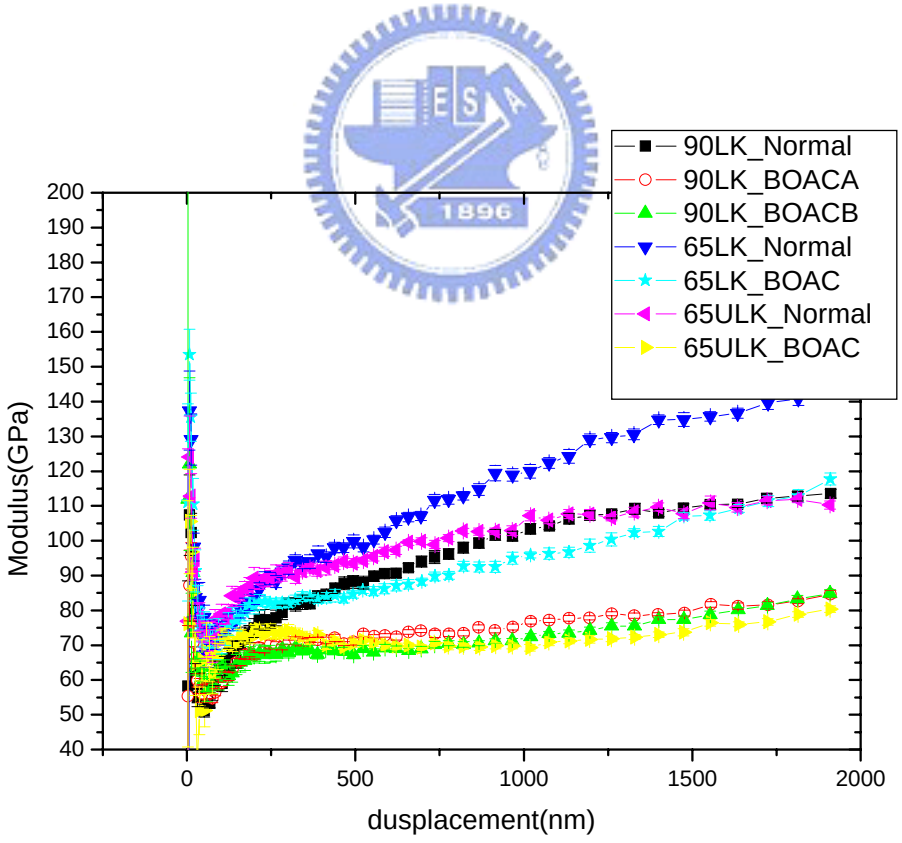

Figure 4.3 Nanoindentation results of all BOAC structures

4.1.2.3 King's model Fitting

King's model, which has been described in the previous chapter, will be used to quantify the mechanical strength of BOAC structures. We took a BOAC structure, for example, 90LKNormal to illustrate the fitting step of $E_f^{\text{nanoindentation}}$. $E_f^{\text{nanoindentation}}$ was the raw data from nanoindentation measurement as shown in Figure 4.4, while the fitting curve related to substrate effect up to 1.2 μm was represented by $E_f^{King's-fitting}$. First E_f of aluminum was measured to complete the $E_f^{King's-fitting}$ fitting and calculate the E_{cs}, which was the modulus of composite BOAC substrate in a two-layered Al/substrate model. We changed E_{cs} and used "try and error" to fit the most matched curve. The E_f of Al was 69.2 GPa as listed in Table 4-1. Therefore, the modulus of the composite substrate in 90LKNormal was 109 GPa from $E_f^{King'sfitting}$ fitting. From Figure 4.4, the range of fitting was only valid between 0 and 1200 nm because King's model fitting was limited to the Al film thickness, which was 1.2 μm in our BOAC structures.

This method was also applied to all BOAC structures with fitting results shown in Figure 4.5 ~ 4.11. Table 4.2 listed the E_{cs} of all BOAC samples. In the later section, we will discuss the learning and issues of such fitting method and the relationship between the E_{cs} and BOAC structures.

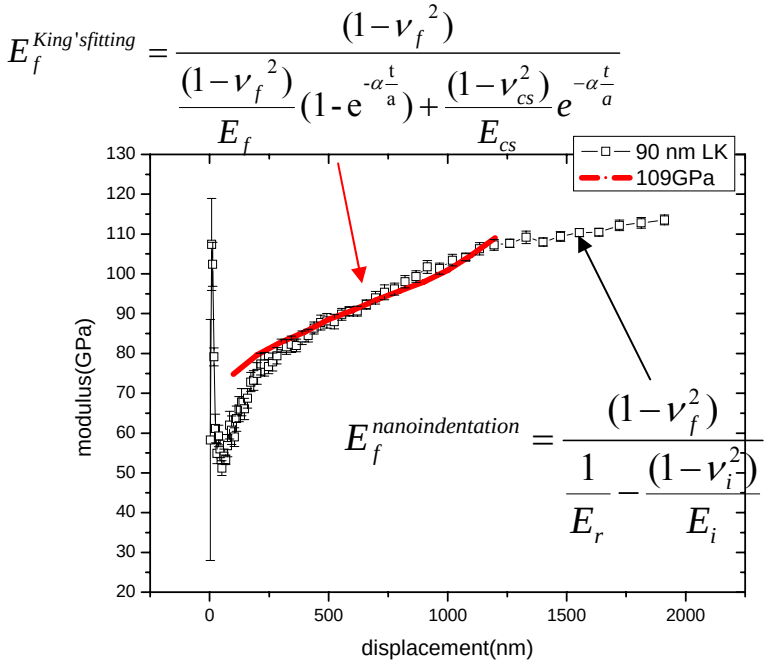

Figure 4.4 Curve fitting of E_f using King's model for displacement below 1200 nm

Table 4.2 Modulus of composite substrate in various BOAC structures

Samples	E_{cs} (Al film/composite substrate), GPa
90LKBOAC A	75.5
90LKBOAC B	70
90LKNormal	109
65LKBOAC	95
65LKNormal	125
65ULKBOAC	71
65ULKNormal	119

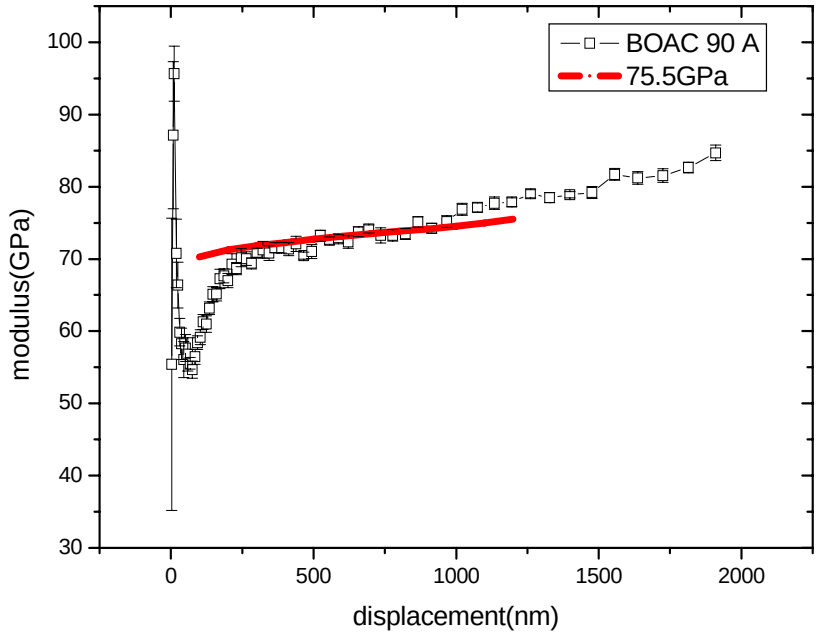

Figure 4.5 King's model fitting result for 90LKBOAC A

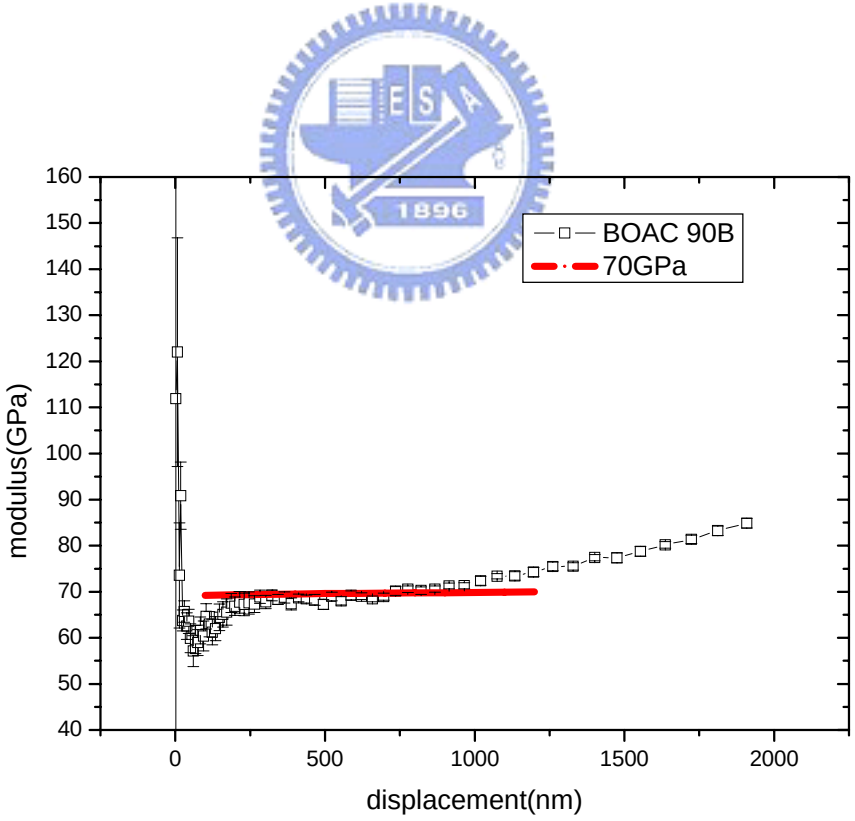

Figure 4.6 King's model fitting results for 90LKBOAC B

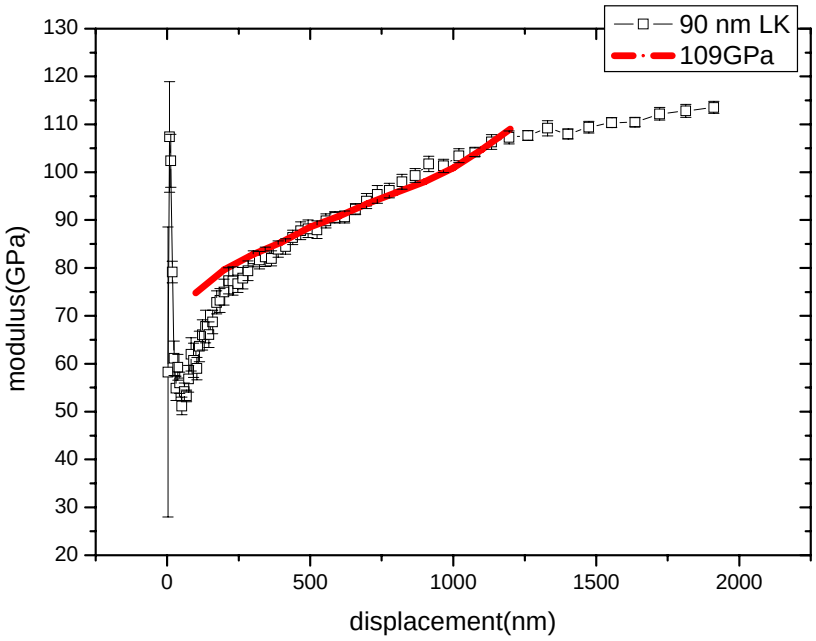

Figure 4.7 King's model fitting result for 90LKNormal A

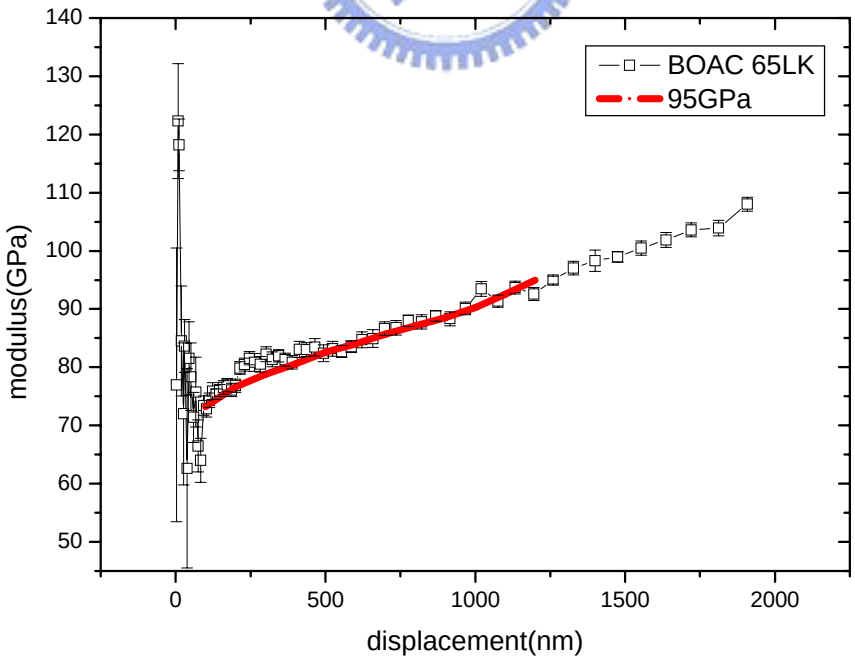

Figure 4.8 King's model fitting result for 65LKBOAC

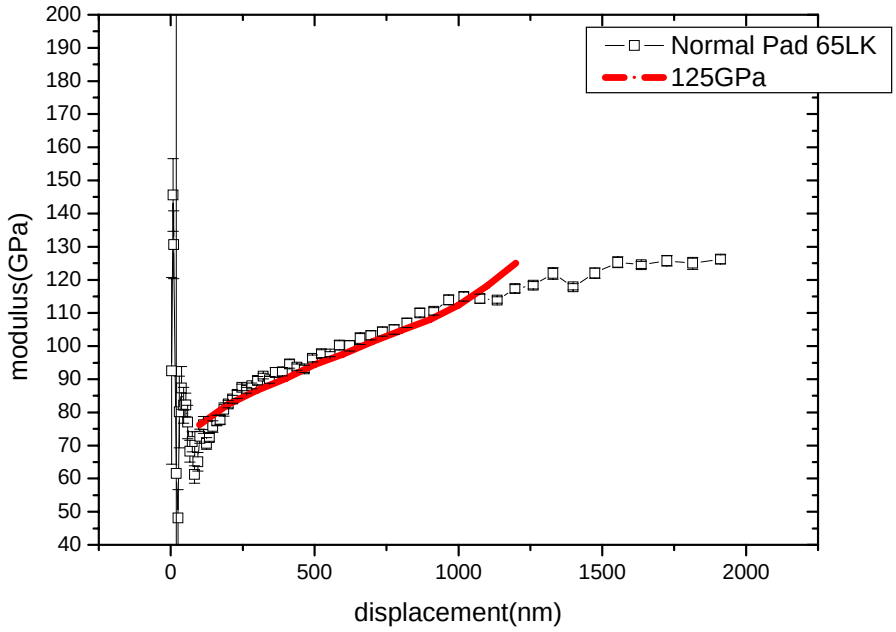

Figure 4.9 King's model fitting result for 65LKNormal

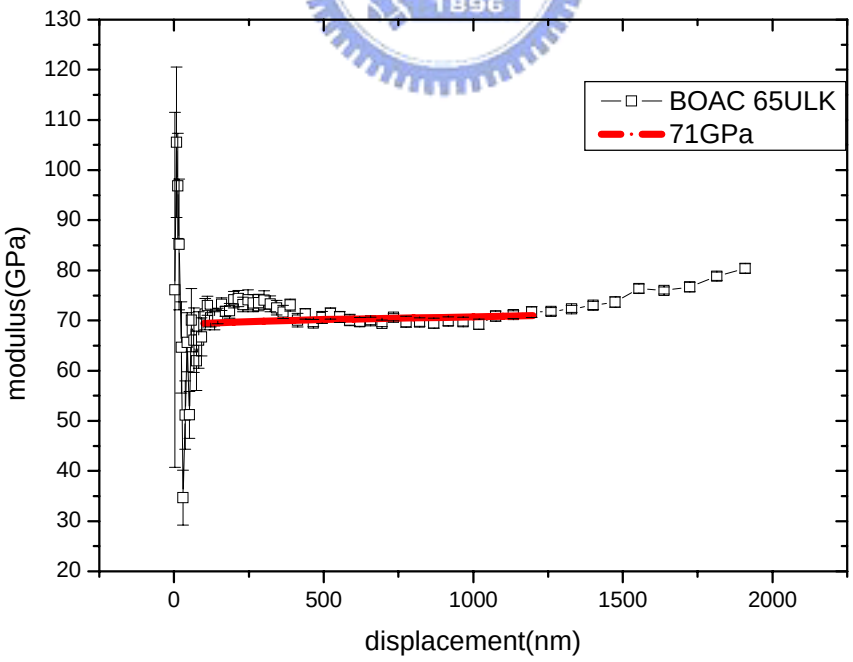

Figure 4.10 King's model fitting result for 65ULKBOAC

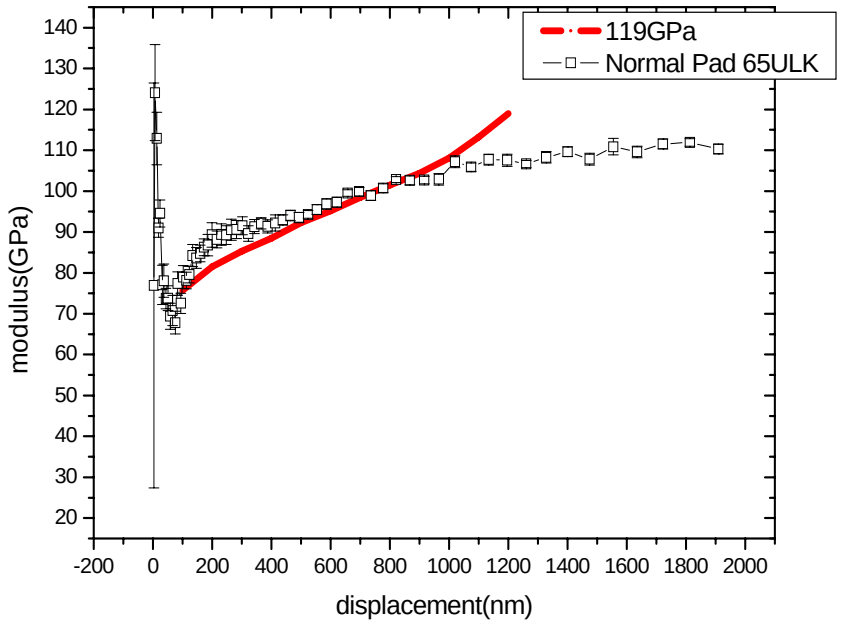

Figure 4.11 King's model fitting result for 65ULKNormal

4.2 Analysis and Discussion

4.2.1 Parameters affecting BOAC mechanical strength

In the previous sections, we have reported the measurement and fitting for 7 different BOAC samples, which included cases for studying the effects of technology nodes, mechanical strength of low-k materials, bond pad structures and copper density of metal lines. The E_{cs}, the modulus of composite BOAC substrate in a two-layered Al/substrate model, will be further analyzed and discuss how these parameters can affect the mechanical strength of BOAC structures.

4.2.1.1 Bond pad structures

From Table 3.2, we took 90LKBOAC A vs. 90LKNormal to analyze how the bond pads affected the mechanical strength of BOAC as illustrated in Figure 4.12. From Table 4.2, the E_{cs} of 90LKBOAC A and 90LKNormal were 75.5 GPa and 109 GPa, respectively. The difference of E_{cs} between these two bond pad structures was 33.5 GPa. This could be attributed to the full array of dummified, stacked trench/via reinforcement in M1-6 in normal pad. In contrast, BOAC contained typical M1-6 lines and via with less than 6% of die area, randomly distributed throughout the die as shown in Figure 4.13. Similar result was observed for normal pad vs. BOAC structure in 65 nm node and design as shown in Figure 4.14. However, normal pad was much stronger than BOAC pad in the case of 65 nm parts. This magnified the need for understanding the mechanical strength of structure underneath the Al pad in the wire bonding process. Although the BOAC structure did not possess mechanical strength as strong as conventional normal pad, it still possessed the basic mechanical strength to resist the impact force from wire boning or wafer probe as judged from their passing in bondability test.

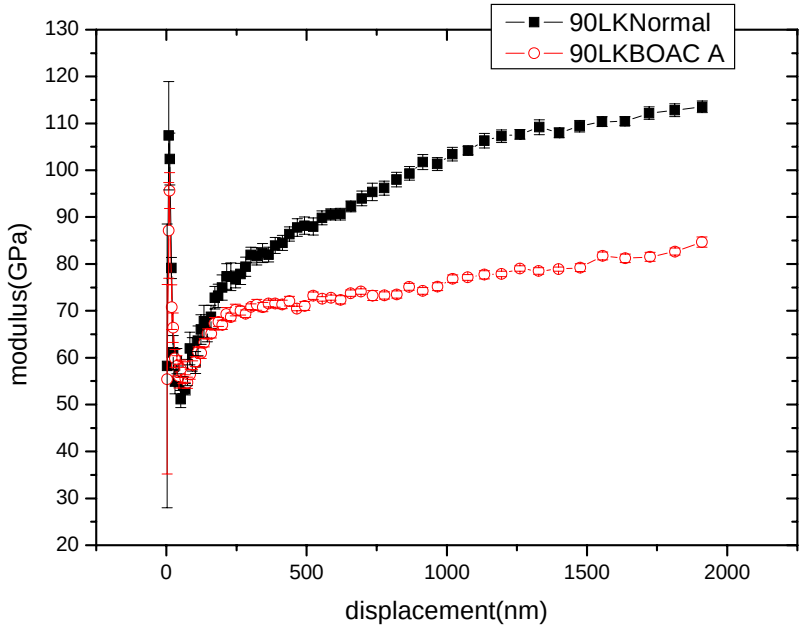

Figure 4.12 Nanoindentation results of 90LKNormal vs. 90LKBOAC A

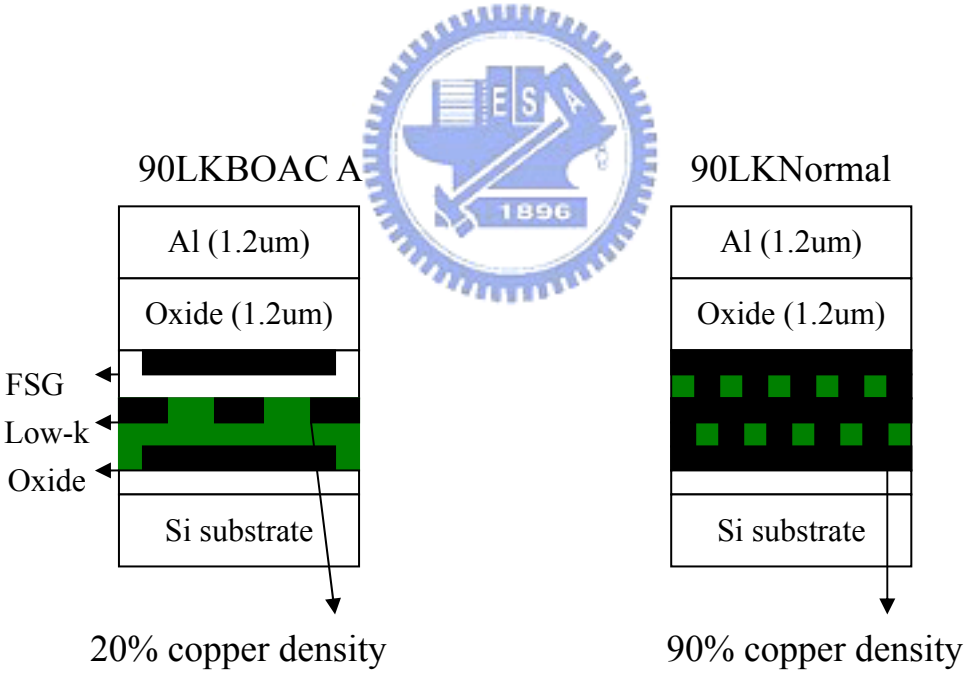

Figure 4.13 Structures of 90LKBOAC A and 90LKNormal

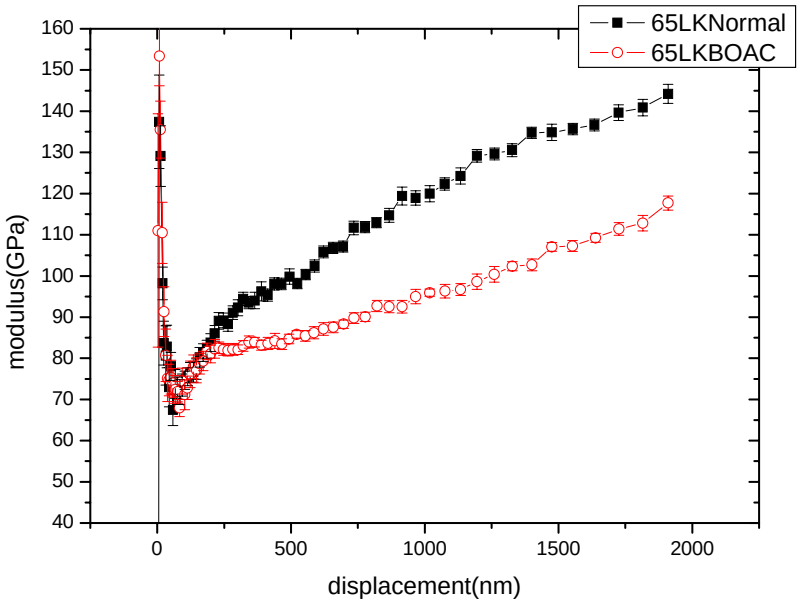

Figure 4.14 Nanoindentation results of 65LKNormal vs. 65LKBOAC A

4.2.1.2 Copper density

Next we investigated how the copper densities affected the mechanical strength of BOAC using 90LKBOAC A vs. 90LKBOAC B listed in Table 3.2 and shown in Figure 4.15. From Table 4.2, the E_{cs} of 90LKBOAC A and 90LKBOAC B were 75.5 GPa and 70 GPa, respectively. The difference in E_{cs} was 5.5 GPa since these two structures were almost the same except top copper densities as shown in Figure 4.16. The top copper densities for 90LKBOAC A and 90LKBOAC B were 90 % (block) and 10 % (ring). The difference of E_{cs} was small although the difference in copper density was large. It indicated that the oxide layer over the top metal layer absorbed the main impact force from indenter, so the top metal's density seemed to have little influence on the mechanical strength of BOAC structures.

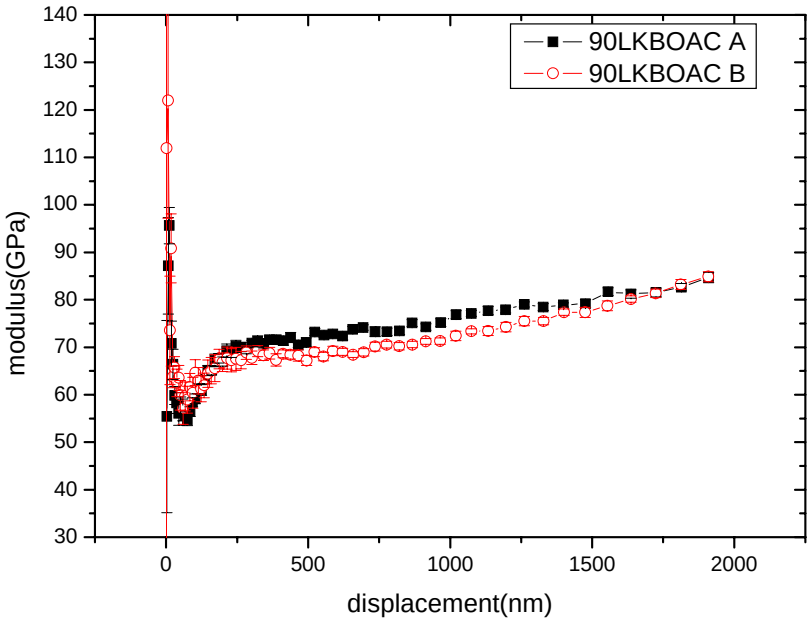

Figure 4.15 Nanoindentation results of 90LKBOAC A vs. 90LKBOAC B

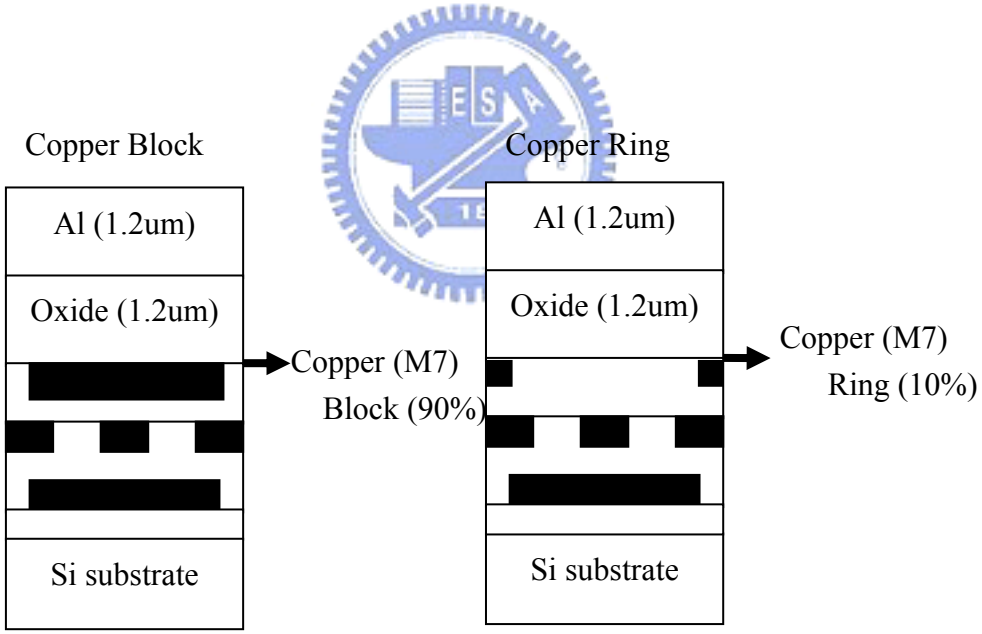

Figure 4.16 The cross-sectional view of M7 copper densities in BOAC structure

4.2.1.3 Technology nodes

We then studied how the backend dimensional scaling affected the mechanical strength of BOAC structures using 90LKBOAC A vs. 65LKBOAC listed in Table 3.2.

The thicknesses of passivation, Al pad and top oxide layer remained the same, while ILD/metal thickness in M1-6 scaled from 90 nm node to 65 nm node with increasing AR in M1-6. From Table 4.2, the E_{cs} of 90LKBOAC A and 65LKBOAC were 75.5 GPa and 95 GPa, respectively. The difference was 19.5 GPa as shown in Figure 4.17. The increased E_{cs} in 65 nm BOAC structire was attributed to the larger Cu fraction in M1-6 layer as illustrated in Figure 4.18, where the Cu fractions in 90 nm and in 65 nm were 44 % and 58 %, respectively. It indicated that the scaling effect had large influence on the mechanical strength of BOAC structures and the higher Cu fraction in the Cu/Low-k layer, the stronger BOAC structure would be.

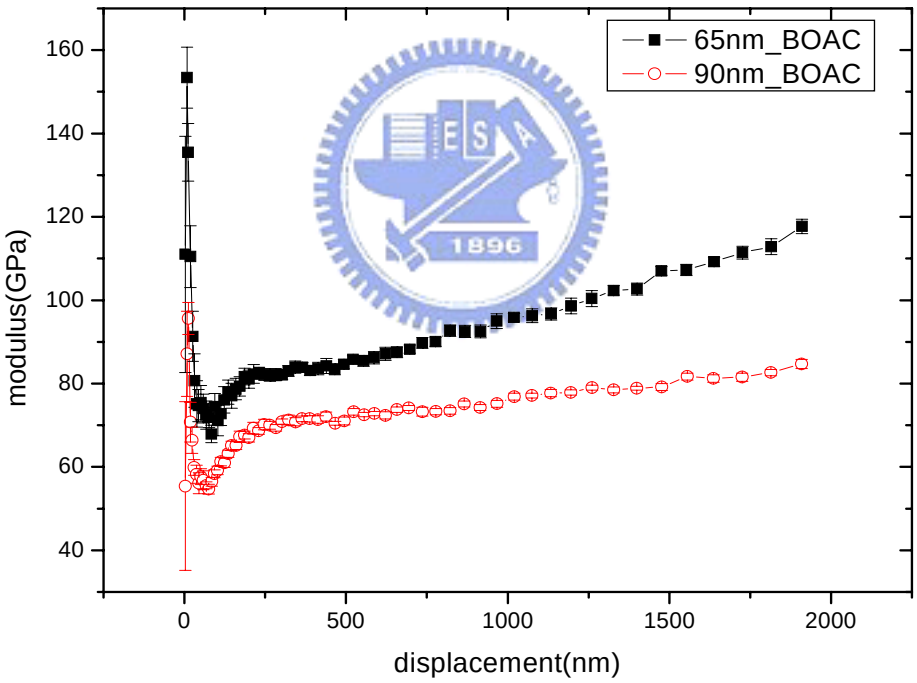

Figure 4.17 Nanoindentation results of 65LKBOAC vs. 90LKBOAC

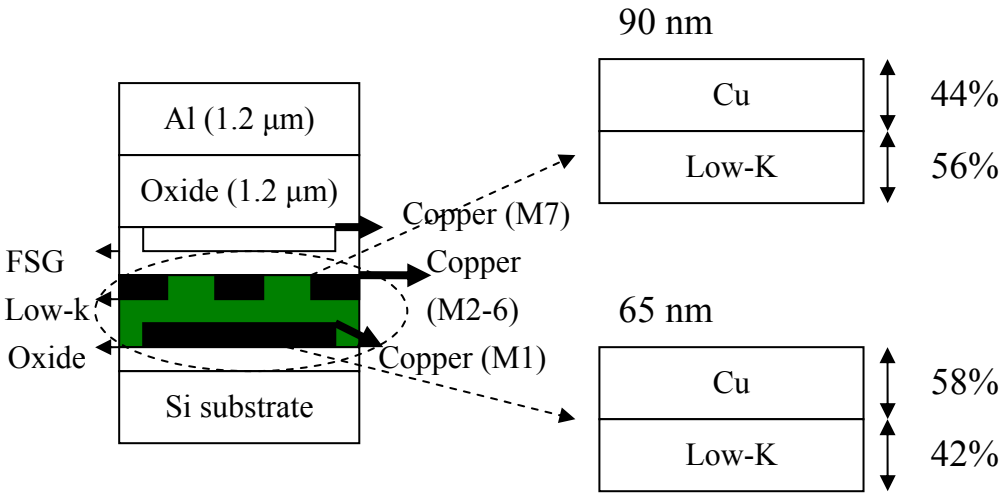

Figure 4.18 Cu fractions in the Cu/Low-k layers of 90 nm and 65 nm structures

4.2.1.4 Low-k materials

We also addressed how the low-k materials affected the mechanical strength of BOAC structures using 65LKBOAC and 65ULKBOAC listed in Table 3.2 and shown in Figure 4.19. These two structures were almost the same except the low-k materials in ILD layer M1-5 as shown in Figure 4.20. From Table 4.2, the E_{cs} of 65LKBOAC and 65ULKBOAC were 95 GPa and 71 GPa, respectively. The difference in E_{cs} (24 GPa) was large, which cannot be sorely attributed to the decrease in ILD's mechanical strength from low-k (15 GPa) in 65 nm to ultra-low-k (9 GPa) in 65 nm parts. Weaker interfacial adhesion in ULK/metal due to the existence of porosity [22, 37] may be the culprit of the much lower E_{cs}. To prove this hypothesis, we used FIB to examine the cross-section of BOAC structures after nanoindentation test as shown in Figures 4.21~4.24. For the low-k sample (LK), there was no crack found under the indentation and the ILD seemed flat except top copper layer. However, in ultra low-k sample (ULK), there were many cracks observed under the indentation and the ILD bended under the impact force. These observations indicated that the ultra low-k materials had low modulus and more importantly weak interfacial adhesion. Other

researcher [37] had shown that the weak adhesion would lower the modulus during nanoindentation. In this study, low modulus and weak adhesion were believed to be the main reasons affecting the mechanical strength of BOAC structures.

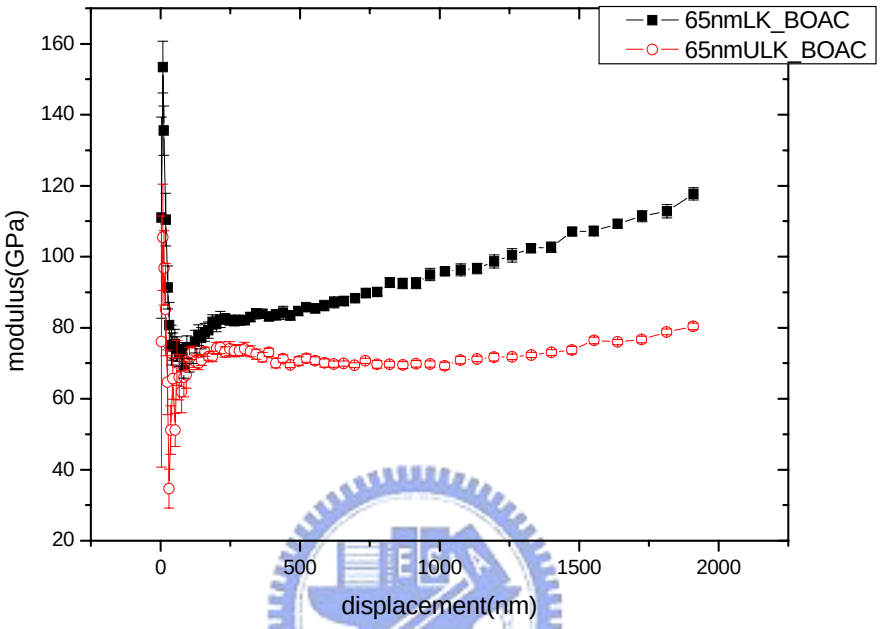

Figure 4.19 Nanoindentation results of 65LKBOAC vs. 65ULKBOAC

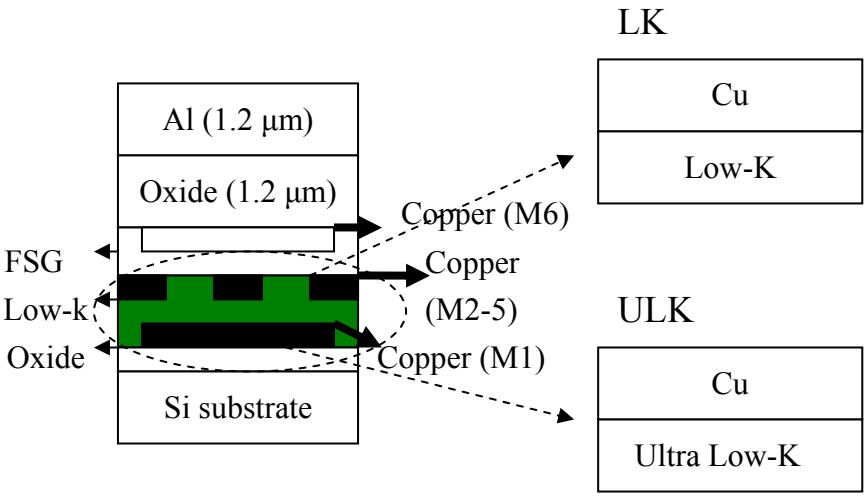

Figure 4.20 Structures of different low-k materials in 65LKBOAC and 65ULKBOAC

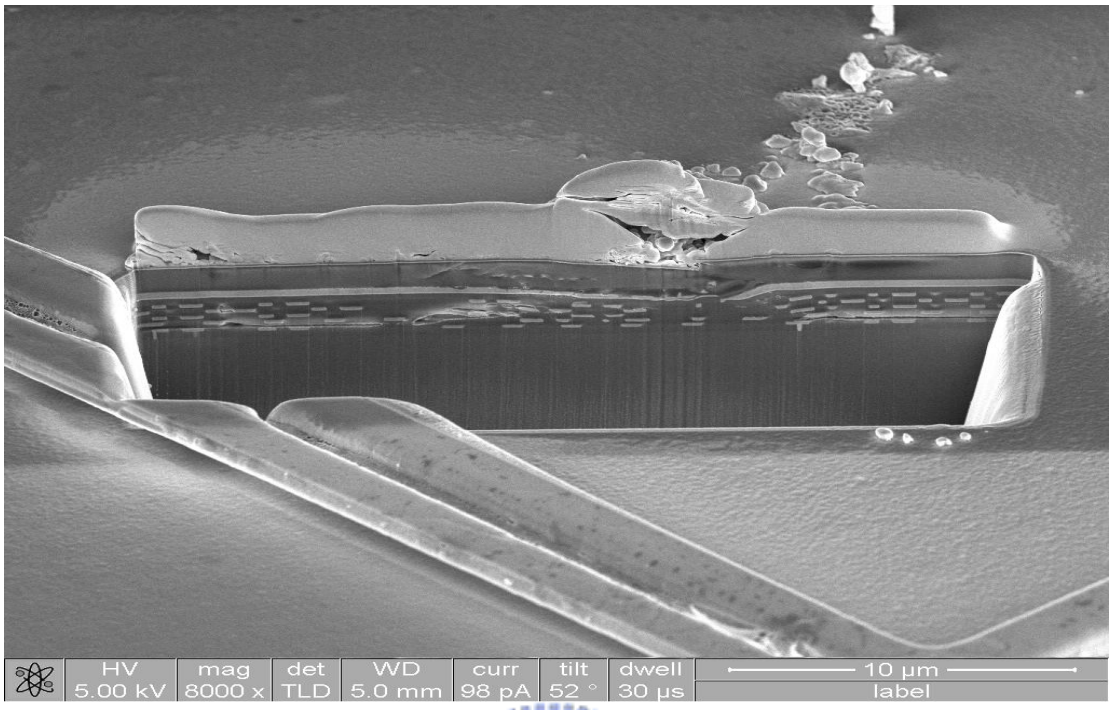

Figure 4.21 FIB cross-sectional view of 65LKBOAC (8,000 X)

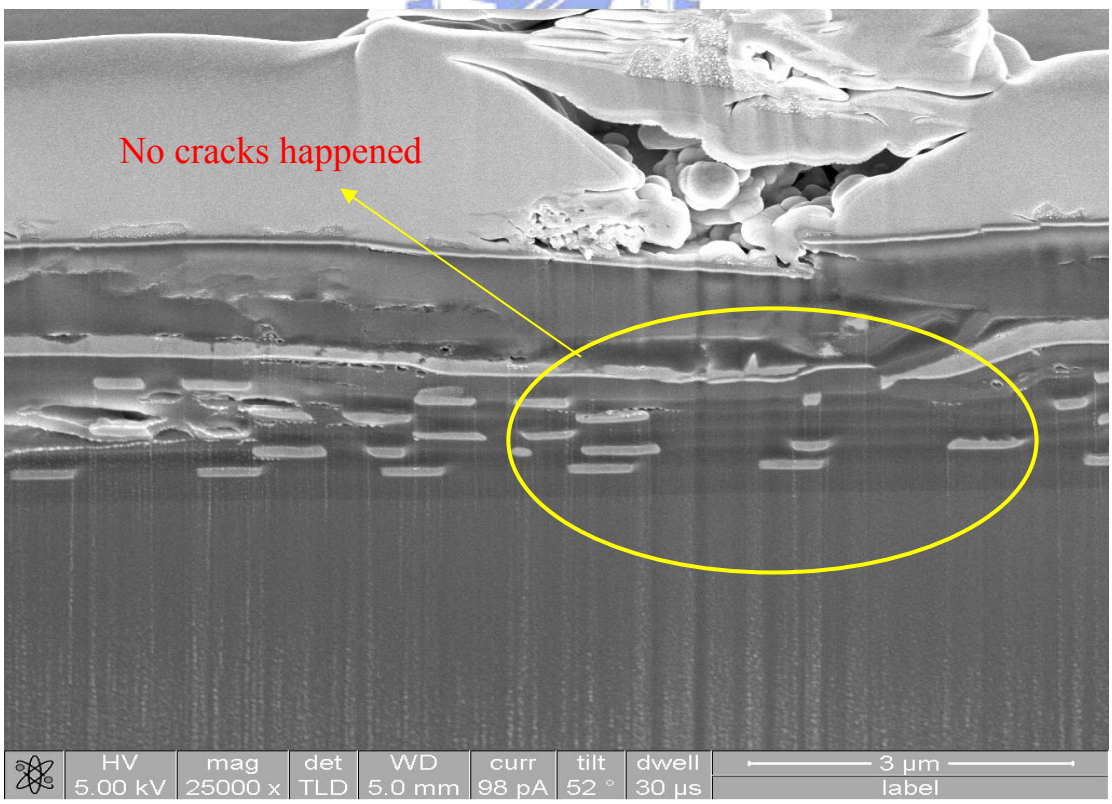

Figure 4.22 FIB cross-sectional view of 65LKBOAC (25,000 X)

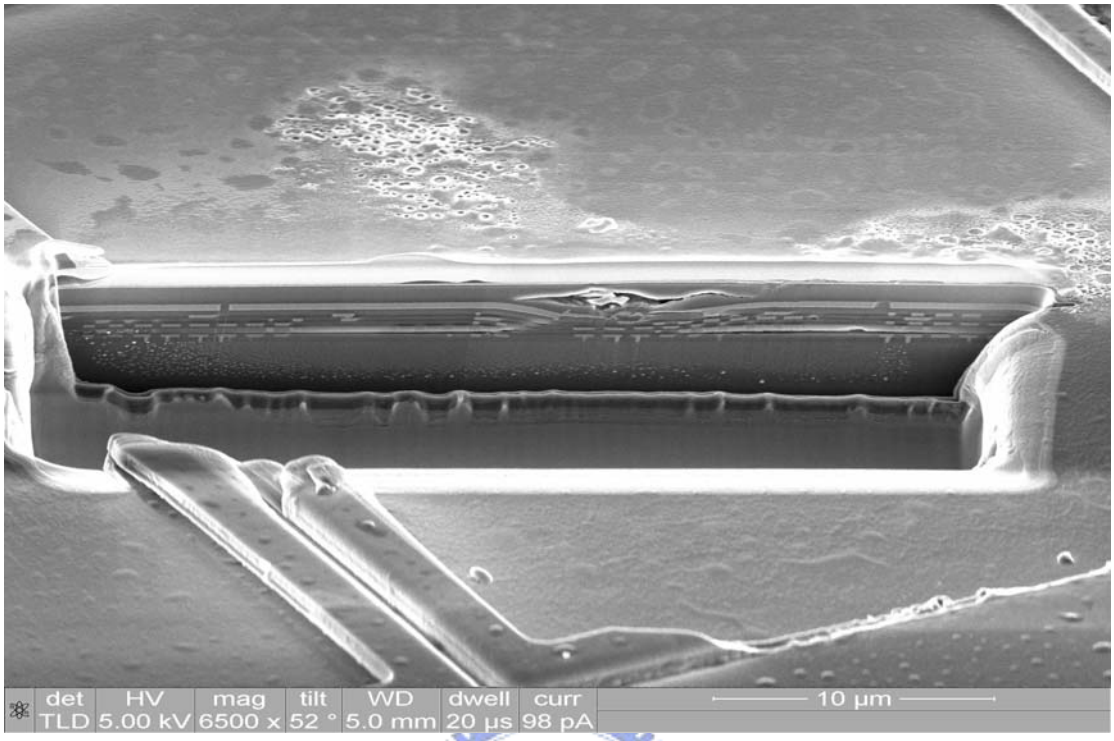

Figure 4.23 FIB cross-sectional view of 65ULKBOAC (8,000 X)

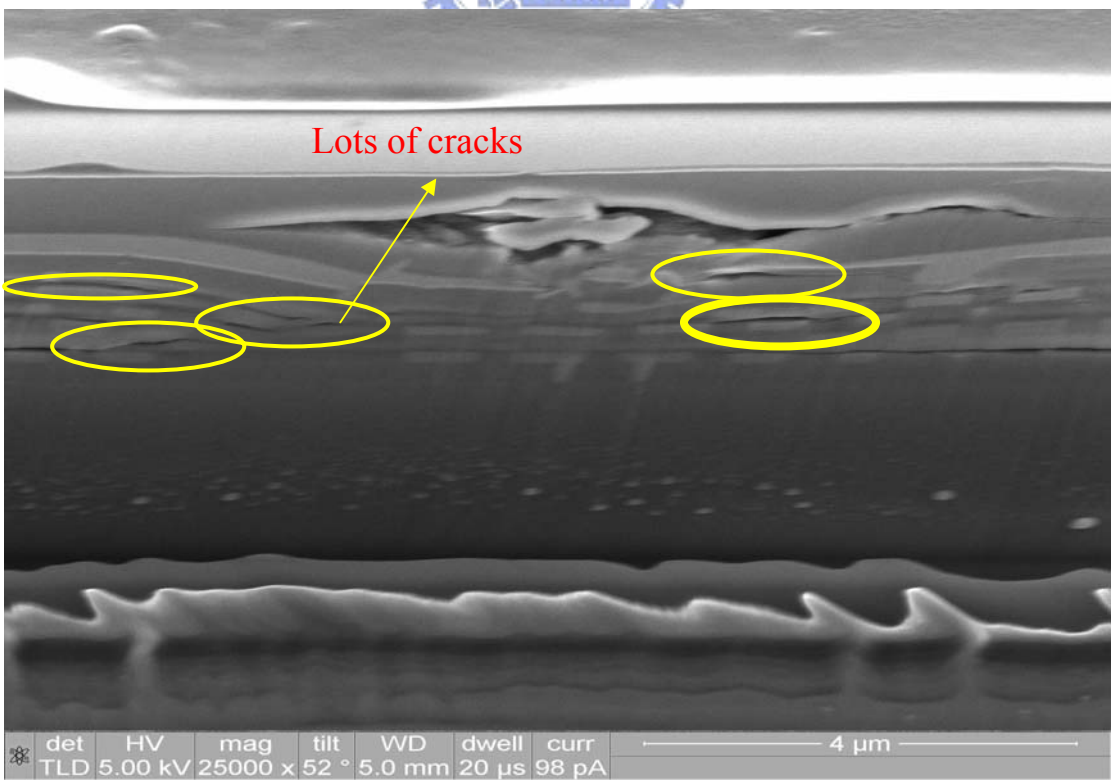

Figure 4.24 FIB cross-sectional view of 65ULKBOAC (25,000 X)

So far, there is no problem using the quantified values to analyze the mechanical strength of various BOAC structures in a soft film/ hard substrate system. However, the accuracy of these quantified values warranted verification. As a result, BOAC structures in a hard film/soft substrate system will be further analyzed to check if the same mechanical strength of BOAC structures can be obtained. In addition, the applicability and issues of these quantified values will be addressed.

4.2.2 Hard film/soft substrate system

When the Al pad was etched from BOAC structures, the stacking of BOAC structures became oxide film/composite substrate structure, which was a hard film/soft substrate system. The nanoindentation results, $E_f^{\text{nanoindentation}}$ of BOAC structure with oxide as the top layer shown in Figure 4.25, decreased with increasing indenter depth, indicating that the moduli of composite BOAC substrates were smaller than the modulus of oxide film. The mechanical strength of composite BOAC substrates in decreasing order was the same as that with the original BOAC structures with Al film on the top.

Curve fitting was also used to characterize the mechanical strength of various BOAC structures with oxide layer on the top. E_f for the oxide film was measured to be 79.5 GPa as listed in Table 4.1. We also changed E_{cs} and used "try and error" to fit the most matched curve. The efficient fitting range was from beginning to the lowest $E_f^{\text{nanoindentation}}$ because the fitting curve $E_f^{King's-fitting}$ didn't rise up in the end of the curve. E_{cs} (Modulus of composite BOAC substrate) for various BOAC structures with oxide on the top can be obtained by curve fitting as illustrated in Figures 4.26-4.32 and summarized in Table 4.3.

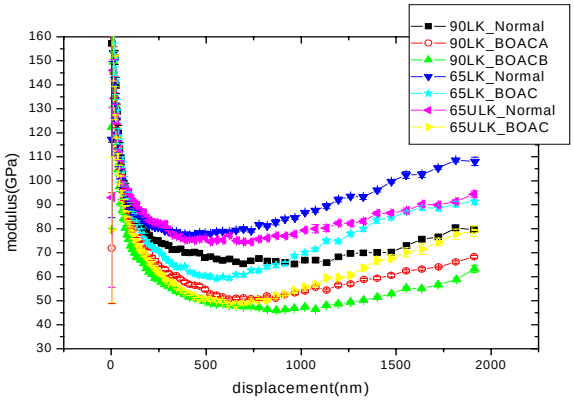

Figure 4.25 Nanoindentation results of BOAC structures with oxide film on the top

Table 4.3 Modulus of composite BOAC substrate with oxide film on the top in a two-layered oxide/composite substrate model

Samples	E_{cs} (oxide film/composite substrate), GPa
90LKBOAC A	45
90LKBOAC B	41
90LKNormal	63
65LKBOAC	54
65LKNormal	80
65ULKBOAC	42
65ULKNormal	74

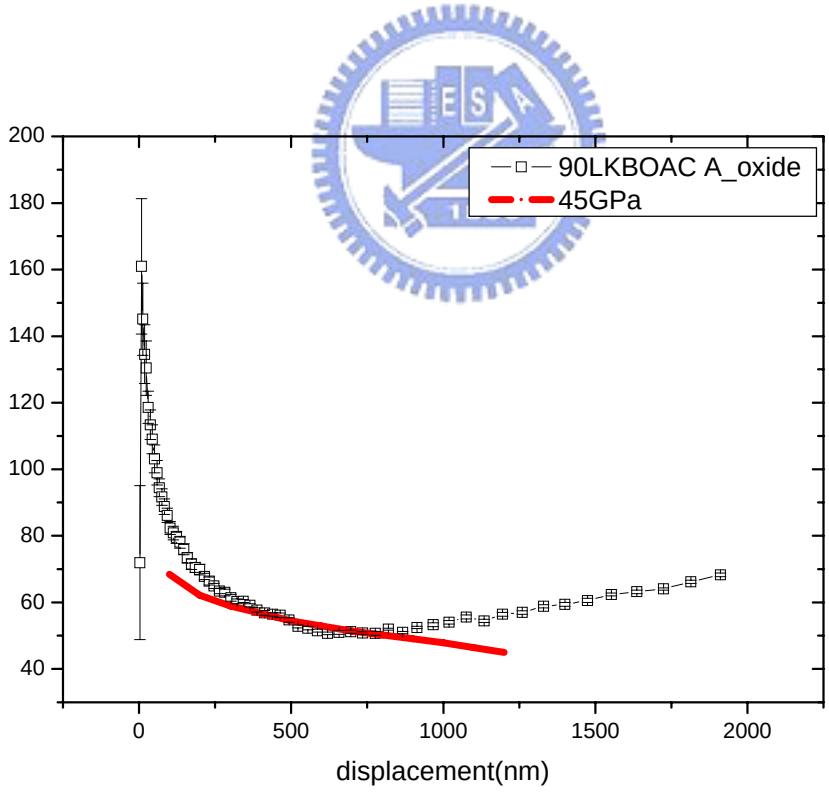

Figure 4.26 King's model fitting result for 90LKBOAC A with oxide film as the top layer

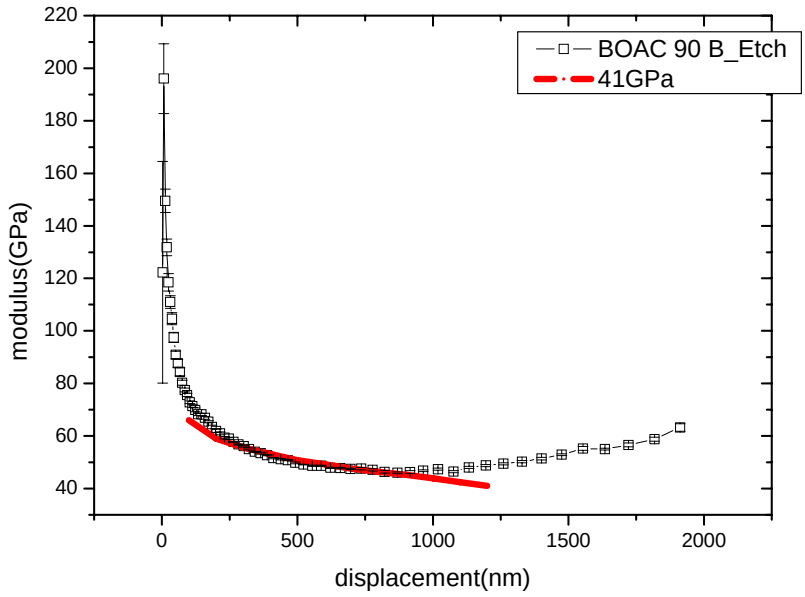

Figure 4.27 King's model fitting result for 90LKBOAC B with oxide film as the top layer

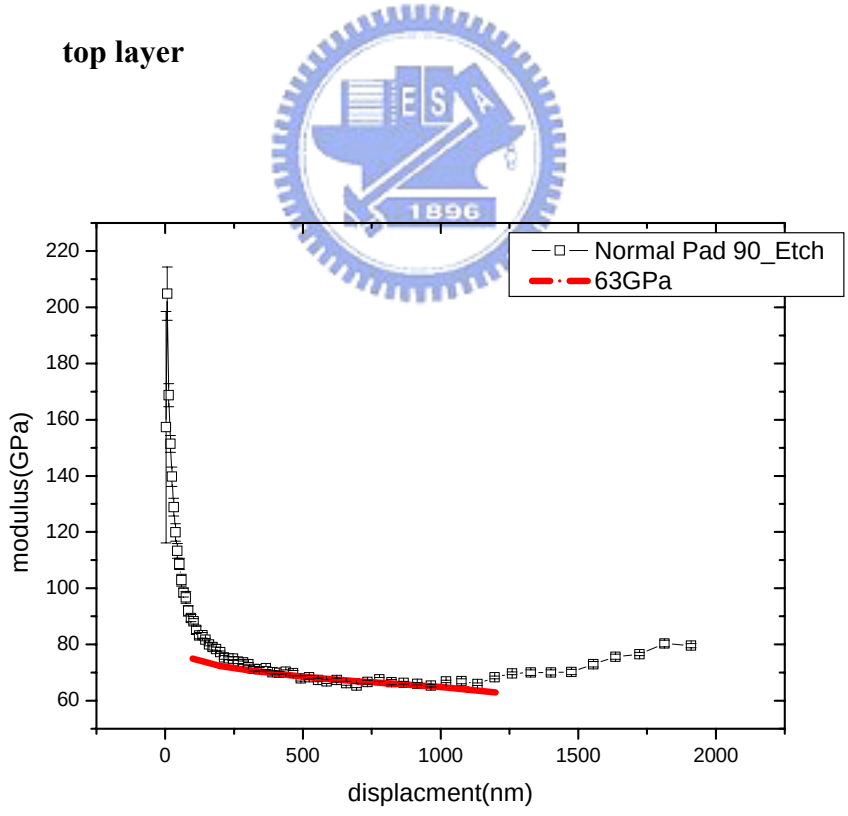

Figure 4.28 King's model fitting result for 90LKNormal with oxide film as the top layer

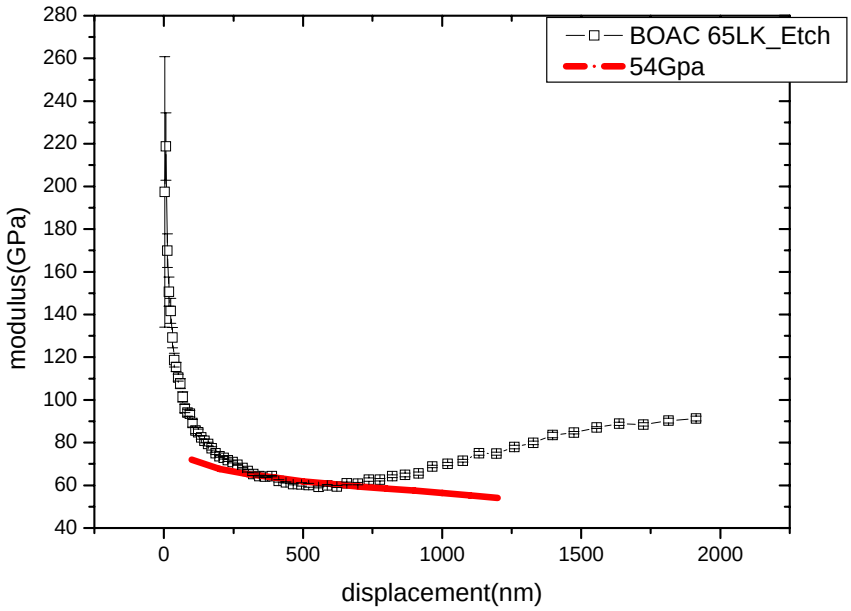

Figure 4.29 King's model fitting result for 65LKBOAC with oxide film as the top layer

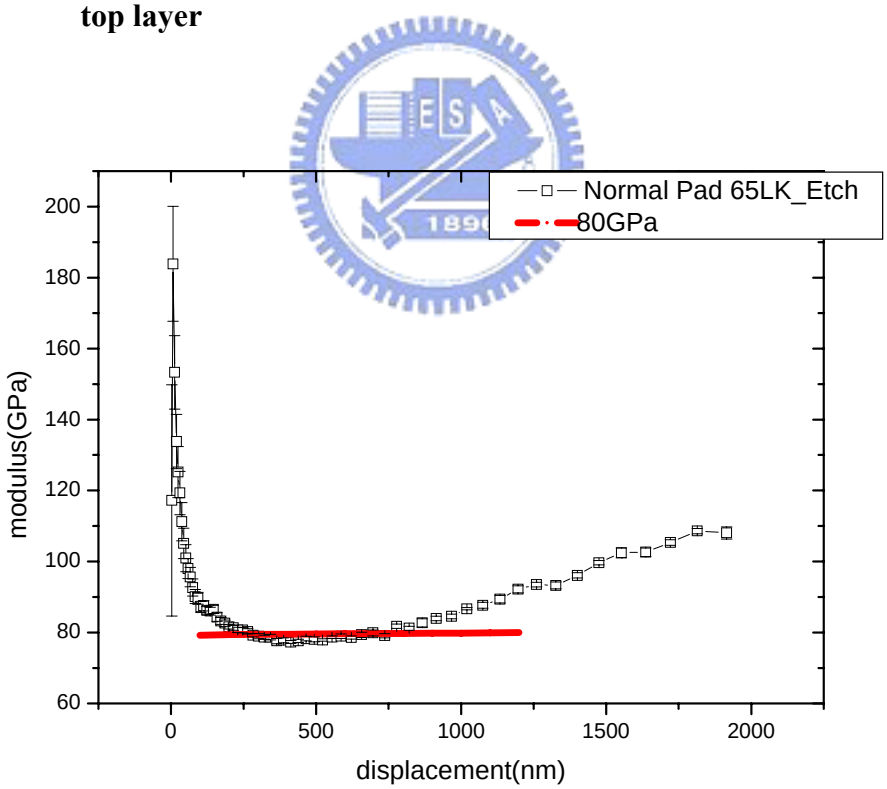

Figure 4.30 King's model fitting result for 65LKNormal with oxide film as the top layer

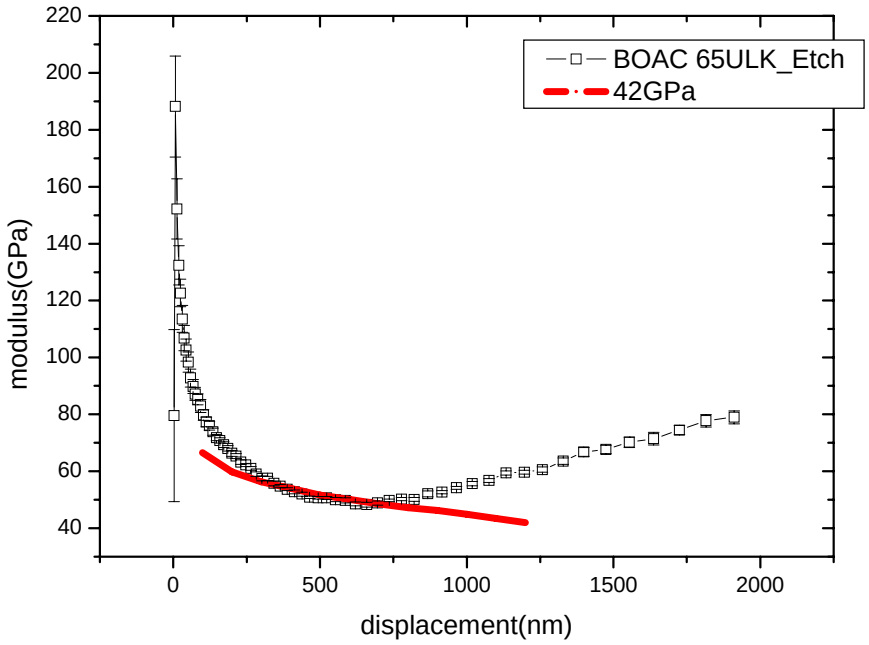

Figure 4.31 King's model fitting result for 65ULKBOAC with oxide film as the top layer

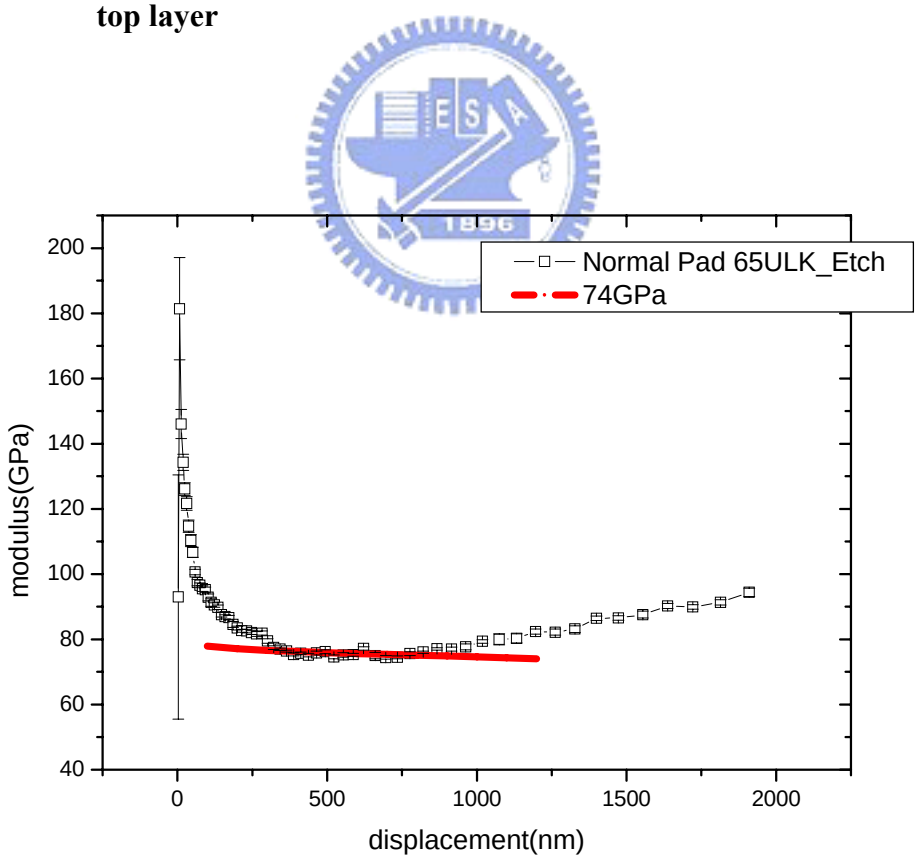

Figure 4.32 King's model fitting result for 65ULKNormal with oxide film as the top layer

Judging from the curve fitting in Figures 4.26-4.32, it was found that significant deviations from $E_f^{\text{nanoindentation}}$ were observed for displacement greater than 700-800 nm. In general, $E_f^{\text{nanoindentation}}$ of BOAC structure with oxide as the top layer, rose up at the displacement near 700-800 nm due to (1) copper/low-k patterned layer underneath oxide layer and (2) the strain-hardening effect. Next we examined the $E_f^{\text{nanoindentation}}$ data between 65 nm parts and 90 nm parts as shown in Figure 4.33. $E_f^{\text{nanoindentation}}$ of 65 nm samples rose up at shorter displacement compared to 90 nm samples because (1) the pitch of each metal layer in Cu/low-k for 65 nm is smaller (0.16 μm vs. 0.32 μm in 90 nm parts) providing more of strain hardening and (2) the thicknesses of the 65 nm samples were thinner than that of 90 nm; thus its affected region touched the hard oxide layer earlier. These two reasons contributed the $E_f^{\text{nanoindentation}}$ of 65 nm parts to rise up earlier than that of 90 nm at the displacement near 700-800 nm.

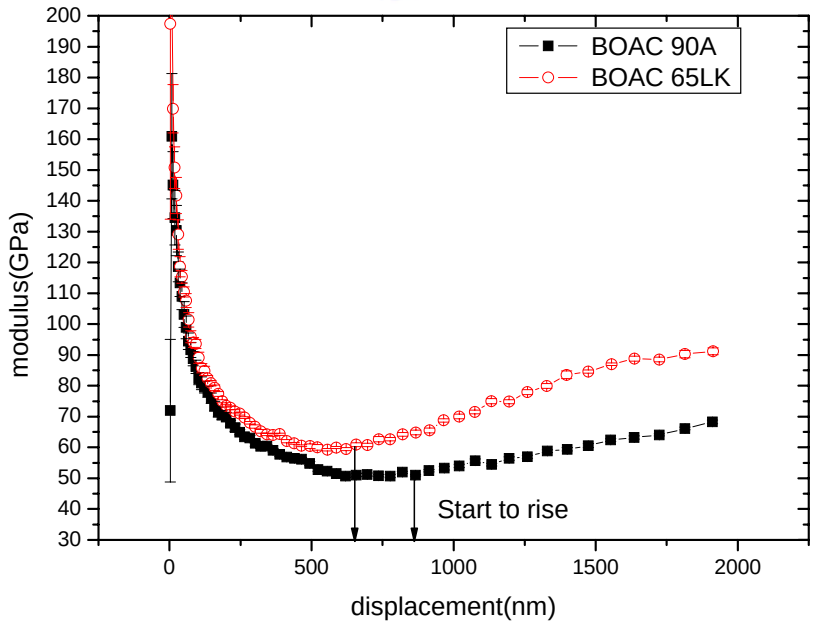

Figure 4.33 Nanoindentation results of BOAC 90A vs. BOAC 65LK with oxide film as the top layer

4.2.3 The difference in E_{cs} between Al film/composite substrate and oxide film/composite substrates

We combined Table 4.2 and Table 4.3 into Table 4.4 for comparison.

Table 4.4 Modulus of composite BOAC substrate (Al vs. oxide)

Samples	E_{cs} (Modulus of composite BOAC substrate), GPa	
	Al film/composite substrate	Oxide film/composite substrate
90LKBOAC A	75.5	45
90LKBOAC B	70	41
90LKNormal	109	63
65LKBOAC	95	54
65LKNormal	125	80
65ULKBOAC	71	42
65ULKNormal	119	74

From Table 4.4, the E_{cs} of oxide film/composite substrate were lower than those of Al film/composite substrates for the same BOAC design. The reasons for such discrepancy may be generalized as follow.

1. **The indentation affected region within the composite substrates was not the same**

For Al film/composite substrate system, the indentation affected region within composite substrates included oxide layer and Cu/low-k layers to a less degree as illustrated in Figure 4.34. In contrast, for oxide film/composite substrate, the indentation affected region within composite substrates included primarily Cu/low-k

layers and to a less degree of Si substrate. Since the modulus of oxide and low-k were 79.5 GPa and 15.4 GPa, respectively, it could be easily understood that the E_{cs} would be larger in the Al film/composite substrate system than that in the oxide film/composite substrate system.

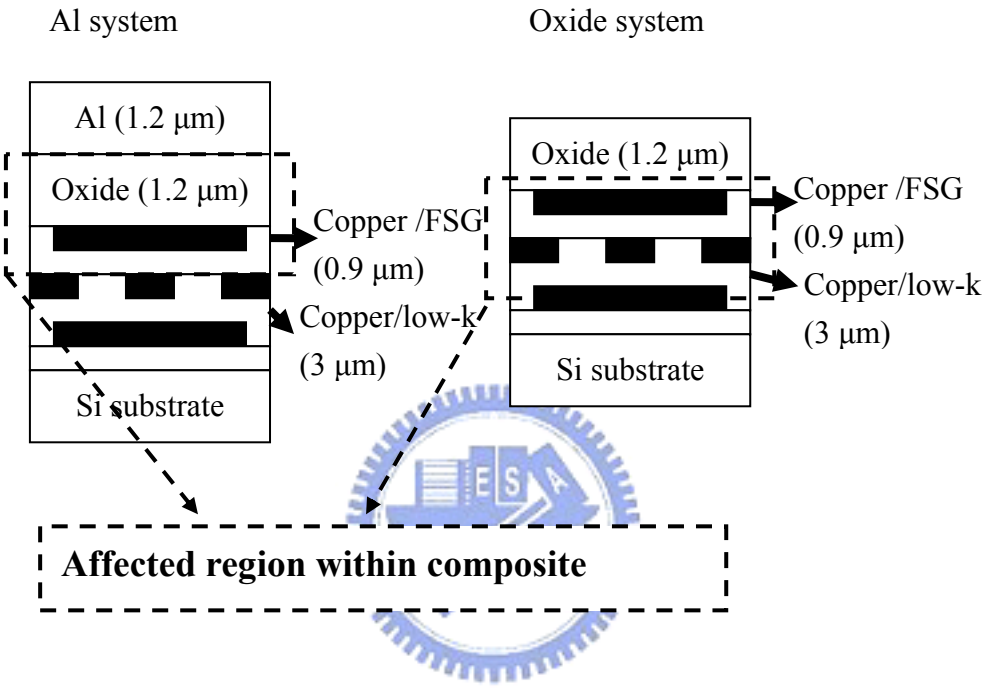

Figure 4.34 The affected regions within the composite substrates

2. The impact force was different in two different film/substrate systems

When the indenter traveled through the film, it needed higher impact force in the oxide film/composite substrate system than that in the Al film/composite substrate system because the oxide film was harder than the Al film. Moreover, high impact force would damage the structures under the impact of indentation; thereby the modulus would be underestimated. As a result, the oxide film/composite substrate would be damaged by impact force more easily than Al film/composite substrate, leading to smaller E_{cs} than Al film/composite substrate.

However, there are two conflicting observations in these two film/substrate systems.

1. There was large discrepancy of the calculated E_{cs} of 65LKBOAC between the Al/substrate system and the oxide/substrate system, namely 95 GPa vs. 54 GPa as listed in Table 4.4. Figure 4.35 showed the relation between these two film/substrate systems. In the Al/substrate, the modulus of oxide was 79.5 GPa and the E_{cs} was 95 GPa, indicating that the modulus of the composite substrate under the oxide layer should be larger than 79.5 GPa, or even 95 GPa. But in the oxide/substrate system, the modulus of the composite substrate under oxide layer, E_{cs}, was 54 GPa, which was not reasonable.
2. In the Al/substrate system, $E_f^{\text{nanoindentation}}$ increased with increasing indenter depth after the indenter penetrated into the oxide layer at the displacement of ≧ 1200 nm as shown in Figure 4.3. It was thought that composite substrate under oxide layer was weaker than the oxide layer, the $E_f^{\text{nanoindentation}}$ should decreased after the indenter penetrated into the oxide layer. Instead, $E_f^{\text{nanoindentation}}$ increased after the displacement ≧ 1200 nm as shown in Figure 4.3, which was not reasonable.

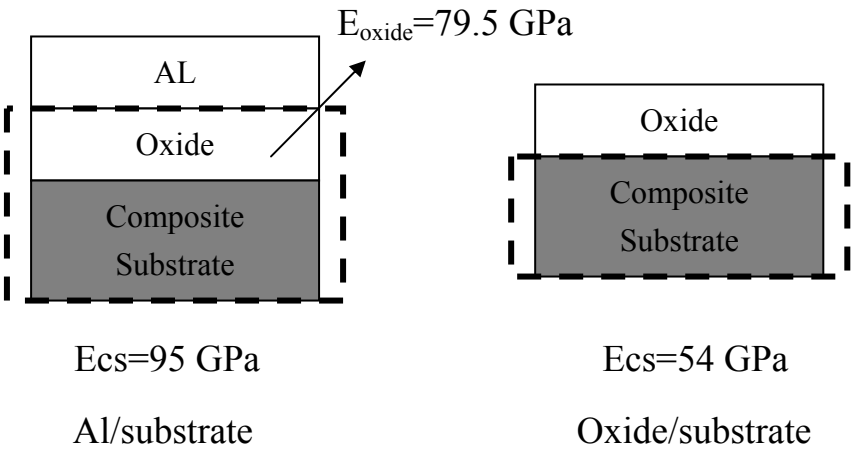

Figure 4.35 Comparison of E_{cs} between different film/substrate systems

The reason for such discrepancies was the contact-area effect induced by the difference in the hardness of materials in the BOAC stack. The contact-area effect will be further discussed in the following section.

4.2.4 The contact area effect

The hardness would affect the modulus during nanoindentation. Researchers [36, 38] found that the hardness would affect the contact area (A) during nanoindentation. Soft films on hard substrates tended to pile-up when indented, while hard films on soft substrates tended to sink-in. Hence the true contact depth was underestimated in the case of a soft film on a hard substrate and overestimated in the case of a hard film on a soft substrate, when compared to the calculated contact depth using the Oliver – Pharr method. Since contact area was a function of contact depth, contact area (A) was underestimated in the case of a soft film on a hard substrate and overestimated in the case of a hard film on a soft substrate. From Equation 3.1 and Equation 3.2, the hardness and modulus would be affected by the contact area (A). For Al film/composite substrate, the E_{cs} would be overestimated while the contact area (A) was underestimated. For the oxide film/composite substrate, the E_{cs} would be underestimated while the contact area (A) was overestimated. The contact area (A) effect and method to eliminate the contact area factor will be discussed in the following section.

4.2.4.1 Eliminating the contact area factor

A method [36, 38] based on P/S^2 was employed to eliminate the contact area by combining Equation 3.1 and Equation 3.2 into Equation 4.1.

$$\frac{P}{S^2} = \frac{1}{\beta^2}\frac{\pi}{4}\frac{H}{E_r^2} \tag{4.1}$$

P/S^2 was directly proportional to hardness H and inversely proportional to the square of the reduced modulus E_r. And the contact area (A) was eliminated in the expression of P/S^2. Since E_s (E_{cs}) was proportional to E_r according to Equation 3.5, we would use this relation to analyze the true modulus during nanoindentation. Figure 4.36 and 4.37 showed the P/S^2 as a function of displacement in the Al film/composite substrate and oxide film/composite substrate samples, respectively.

For Al film/composite substrate samples, P/S^2 was inversely proportional to the square of the reduced modulus E_s (E_{cs}), implying that lower values of P/S^2 meant higher E_{cs}. From Figure 4.36, P/S^2 of 65 nm samples were lower than those of 90 nm samples at about 200 nm displacement depth, indicating that E_{cs} of 65 nm samples were higher than those of 90 nm samples at the initial stage as described in the previous section. The P/S^2 increased as the depth increased from about 200 nm to 1100 nm depth. This was caused by the changing E_{cs} as the affected region moving from stiff oxide layer down to more of weak low-k layers with the increasing indenter depth. Since composite substrate was composed of oxide/M1-6 layers with low-k and different pattern density, such composite substrate was not uniform, but exhibited a continually changing substrate with increasing indenter depth through different layer in the stack. For BOAC structures using 90 nm technology such as 90LKBOAC A and 90LKBOA B which had the same layout in the copper/low-k layers, the increasing slopes between 200 nm to 1100 nm depth were almost the same. This result was the same for normal pad structures with different low-k materials such as 65LKNormal and 65ULKNormal because bond pad strength was primarily supported by the Cu/dielectric layer with 90 % copper density even though the low-k material was very different. Toward the end of 1000 nm depth, the low-k material had little

influence on P/S^2 that 65ULKNormal sample increased a little for lower modulus of ultra low-k. For the 65LKBOAC and 65ULKBOAC, obvious difference in the postive slopes was observed, which was caused by the large difference in modulus between ULD and LK materials while the Cu/low-k layers were mainly supported by the low-k materials in these two BOAC samples. The P/S^2 of 65ULKBOAC increased faster than 65LKBOAC because 65ULKBOAC had lower modulus in Cu/ULK layers. After 1100 nm depth, positive slopes were also observed for all samples, presumably affected by the hardness of the stiffer substrates**.** From Table 4.1, the hardness of oxide and Al were 7.8 GPa and 0.25 GPa. The oxide layer under the Al film was much harder than the Al film. As the indenter penetrated into to the oxide layer after about 1200 nm depth, the P/S^2 increased in different slope due to the hardness of stiffer, oxide layer.

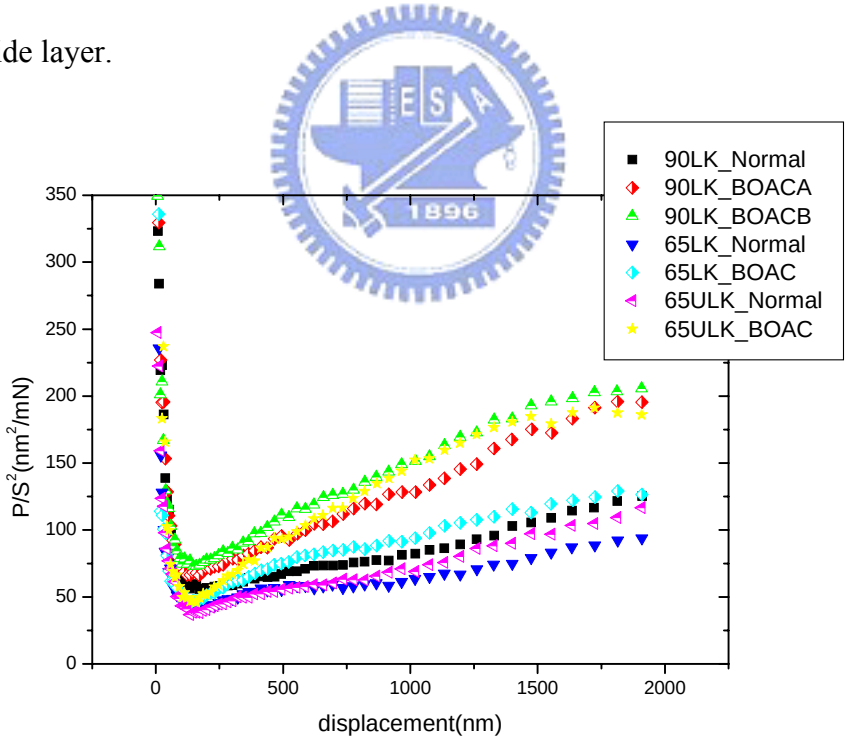

Figure 4.36 P/S^2 as a function of displacement for Al/substrate BOAC structures

In oxide film/composite substrate system, P/S^2 was inversely proportional to the

square of the reduced modulus E_s (E_{cs}). The higher values of P/S^2 meant the lower E_{cs}. From Figure 4.37, the P/S^2 of normal pad samples were lower than those of BOAC samples at about 500 nm depth, implying that E_{cs} of normal pad samples were higher than those of BOAC samples around 500 nm depth, which had been discussed in the previous sections. The P/S^2 values then decreased at depth $>$ 500 nm because of the following two reasons.

1. E_{cs} changed to larger value as the affected region expanded to hard oxide layer and Si substrate beneath the Cu/low-k layers when the indenter traveled downward. For the 65LKBOAC and 65ULKBOAC, the P/S^2 values became the same after 500 nm displacement depth because the contribution from low-k decreased while the affected region included more of the stiffer, oxide layer and Si substrate.
2. Second reason was the hardness effect. In Al film/composite substrate, the hardness effect took place when the indenter penetrated into the substrate. But in oxide film/composite substrate, the hardness effect happened before the indenter penetrated into the substrate. Al film/composite substrate system was characterized as a soft film/hard substrate system where the hard substrate was not affected by the deformation behavior and the soft Al film is accommodating all the plastic deformation until the indenter is close to the film/substrate interface. From Table 4.1, the hardness of oxide and copper (copper was under the oxide) was 7.8 GPa and 1.13 GPa, respectively. Therefore, the oxide film/composite substrate was a hard film/soft substrate system. When the soft substrate yielded at about 500 nm depth, the effective hardness decreased; thus P/S^2 decreased.

Here, 90LKBOAC A and 90LKBOAC B in Al film/composite system were used to illustrate such trend. These two samples did not show significant differences because

in their BOAC structures were almost the same except the top copper metal layer. As shown in Figure 4.38, the top copper metal was a block copper in 90LKBOACA and a copper ring in 90LKBOACA. In oxide film/composite substrate system, the materials under the oxide layer were copper and FSG for 90LKBOACA and 90LKBOAC B samples. From Table 4.1, the hardness of copper and FSG were 1.31 GPa and 6.68 GPa, respectively. As a result, the effective hardness was higher in 90LKBOACB (FSG) than in 90LKBOAC A (copper); thereby P/S^2 of 90LKBOACB (FSG) was higher at about 500 nm depth of displacement.

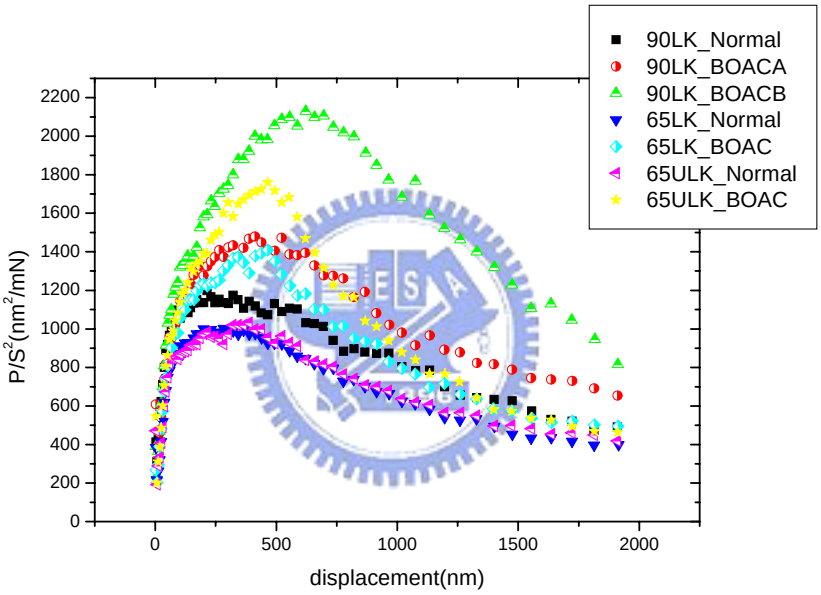

Figure 4.37 P/S^2 as a function of displacement for BOAC structures with oxide as the top layer

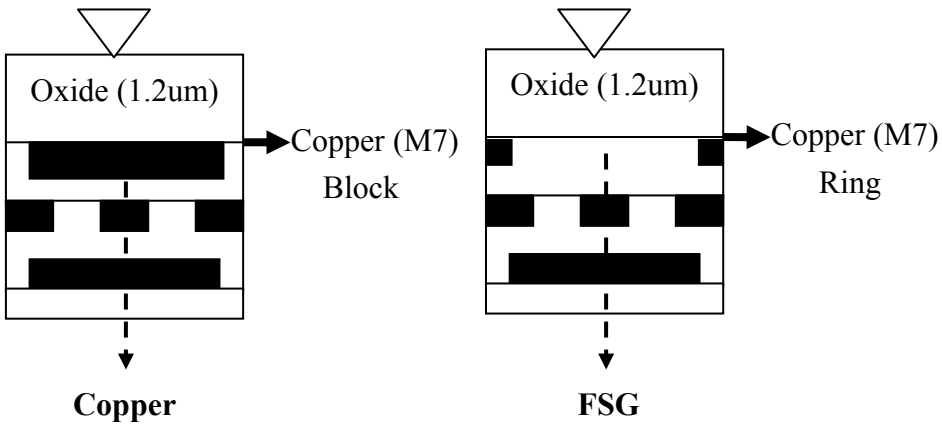

Figure 4.38 The materials and layout under oxide layer for 90LKBOACA and 90LKBOAC B

We then evaluated the E_r excluding the hardness effect by using a constant H(E) and substituting Equation 4.1 into Equation 4.2:

$$E_r = \sqrt{\frac{1}{\beta^2}\frac{\pi}{4}\frac{S^2}{P}H(E)} \tag{4.2}$$

where H(E) for Al was 0.6 GPa [36] while H(E) for oxide was 7.8 GPa obtained in our Laboratory. The results were showed in Figures 4.39 and 4.40.

For Al film/composite substrate system, E_r showed the changing substrate with increasing indenter depth, indicating that the composite substrates is not uniform in the direction of indentation. Comparing to Figure 4.3, $E_f^{\text{nanoindentation}}$ was overestimated, while the calculated values listed in table 4.2 were also overestimated. This elucidates the problem encountered and mentioned in section 4.2.3.

In oxide film/composite substrate system, Er also seemed different as compared to those shown in Figure 4.25. The contact area effect enlarged the difference among different BOAC structures although the trend of their mechanical strength was still the same.

Even though there was expectation to quantify the E_{cs} from Figure 4.39, there was no fitting curve method for a three-layered system, i.e. the soft film-hard layer-soft substrate system yet. However, it is still useful to use the overestimated, calculated values from Table 4.2 to predict if the BOAC structures can pass the bondability test because their trend was the same with the true modulus as shown in Figure 4.39. A modification of King's model will be needed if the exact modulus of the multi-layered substrates is sought after. A model based on multi-layered substrate will be a topic for future study.

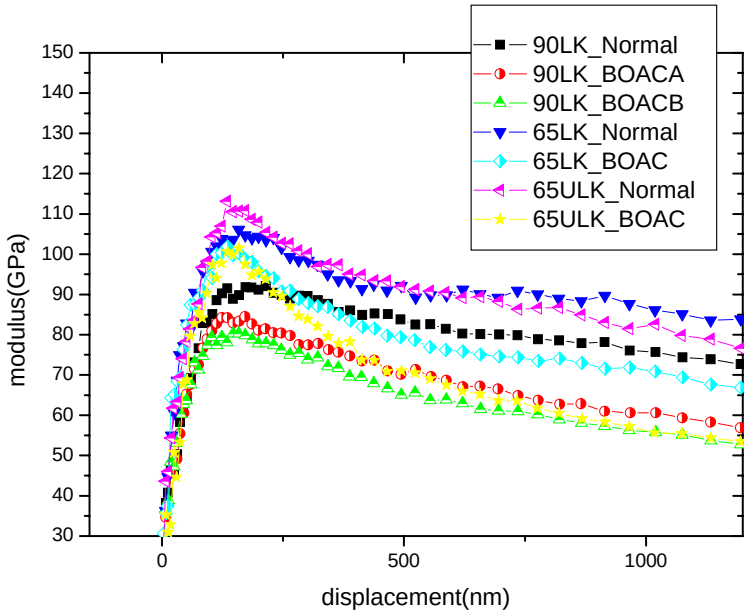

Figure 4.39 E_r excluding the hardness effect of BOAC structures with Al film as the top layer

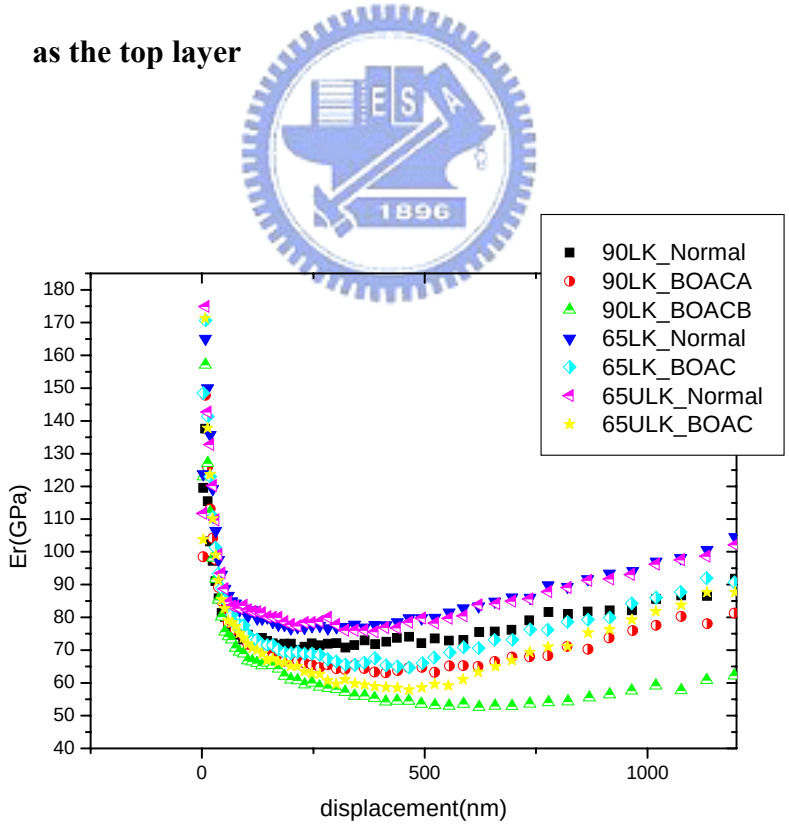

Figure 4.40 E_r excluding the hardness effect of BOAC structures with oxide as the top layer

4.3 Model of mechanical strength in BOAC structures

The calculated values of substrate modulus were overestimated when E_{cs} was used without excluding the contact area effect (hardness effect) because the substrate actually is not a uniform matrix, instead a multilayered metal/low-k structure. Here we attempt to exclude the contact area effect to build a model that can fit the E_r's results as shown in Figures 4.39 and 4.40. We treated a typical BOAC structure as a 3-layered model as schematically illustrated by Figure 4.41. From Figure 4.39 in Al/composite substrate system, the E_r first increased to the maximum and decreased with increasing indenter depth. It is believed that the middle hard layer induced the increase of E_r to the maximum, then the soft composite substrate underneath the oxide layer caused the decrease of E_r after indentation affected region reaching the soft composite substrate.

From Figure 4.40 in oxide/composite substrate system, E_r first decreased to the minimum and increased with increasing indenter depth increasing, indicating that the soft composite substrate was softer than the oxide layer in the initial indentation stage and later the increase of E_r was induced by Si substrate after indentation affected region reaching the hard Si layer. Because the composite substrate is a multilayered copper/low-k structure with different layout and varying mechanical characteristics as the indenter depth increases, we could not evaluate the exact mechanical strength of the substrates using King's model which assumed a homogeneous and uniform substrate. Instead, we attempted to quantify the modulus of the soft composite substrate in experimental observations and theoretical calculation.

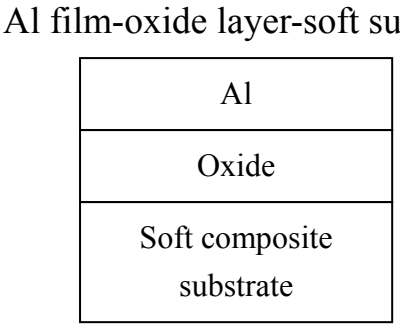

Figure 4.41 Schematic diagram of a 3-layered BOAC model

First we evaluated the modulus of the soft composite substrate from the basic structures using the theoretical calculation from the modulus equation of composite material, Equation 4.3:

$$E_{cs} = x_1 \times E_1 + x_2 \times E_2 + \ldots + x_n \times E_n \quad \ldots\ldots. (4.3)$$

where

X_n = Volume fraction of n material

E_n = Modulus of n material

Figure 4.42 showed the fraction of each layer in soft composite substrate and the modulus of each layer was summarized in Table 4.1. Table 4.5 showed the results by using the theoretical values from the modulus equation of composite material.

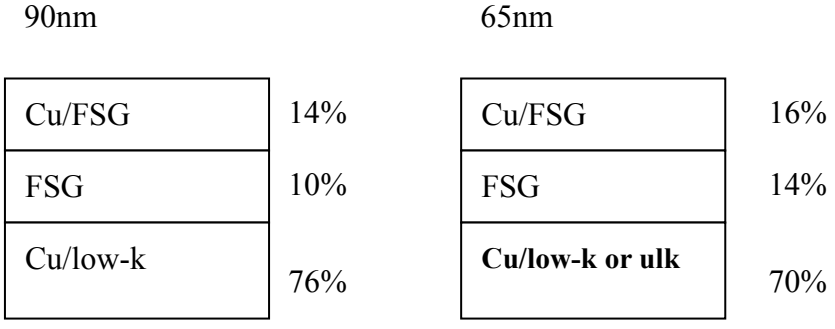

Figure 4.42 Fraction of each layer in the soft composite substrate

Table 4.5 The results by using the theoretical calculation from the modulus equation of composite material.

Samples	Cu/FSG (GPa)	fraction	FSG (GPa)	fraction	Cu/low-k (GPa)	fraction	Total (GPa)
90LKBOAC A	130	0.14	64	0.1	26	0.76	**44**
90LKBOAC B	71	0.14	64	0.1	26	0.76	**36**
90LKNormal	84	0.14	64	0.1	58	0.76	**62**
65LKBOAC	130	0.16	64	0.14	30	0.7	**51**
65LKNormal	84	0.16	64	0.14	72	0.7	**73**
65ULKBOAC	130	0.16	64	0.14	24	0.7	**47**
65ULKNormal	84	0.16	64	0.14	68	0.7	**70**

We used two methods to compare the mechanical strength of BOAC structures, namely (1) Theoretical calculations: the modulus equation of composite material and (2) Experimental observations: E_r excluding contact area effect as shown in Figures 4.39 and 4.40.

In Figure 4.39 of Al film/composite substrate, we assumed the E_r around 1200 nm depth was the modulus of soft composite substrate without oxide layer. In Figure 4.40 of oxide film/composite substrate, we assumed the E_r in the minimum was the modulus of soft composite substrate without oxide layer.

From the results summarized in Table 4.6, we found the values from the equation of composite material E_r were lower than those observed in Figure 4.39 and Figure 4.40. The lower values in theoretical values may be due to underestimate the contribution of top harder layer in soft composite substrate such as Cu/FSG and the strain-hardening induced by the Cu in copper/low-k layers. Moreover, the difference

of E_{cs} between LK and ULK samples such as 65LKBOAC vs. 65ULKBOAC appeared to be larger (in Figure 4.39 and Figure 4.40) than in the theoretical calculation from the equation of composite material. This is because we cannot take weak adhesion due to porosity into account in the theoretical calculation. Instead, it appeared in the experimental results as shown Figure 4.39 and Figure 4.40.

Table 4.6 E_{cs} obtained from two different methods

Samples	E_{cs}		
	Using Er which eliminated the contact area effect (GPa)		Using the modulus equation of composite materials (GPa)
	Al film	Oxide film	
90LKBOAC A	56	63	44
90LKBOAC B	52	52	36
90LKNormal	72	72	62
65LKBOAC	66	65	51
65LKNormal	83	78	73
65ULKBOAC	53	57	47
65ULKNormal	76	75	70

Since E_{cs} changed with increasing indenter depth for BOAC structures consisting Al pad/oxide and copper/low-k multi-layered interconnects, it is difficult to use one value to quantify the mechanical strength of BOAC structures. However, we have proposed two simple models, namely (1) the modulus equation of composite materials (GPa) and (2) Er without contact area effect to simulate experimental data. We found that the tendency of mechanical strength in each BOAC structure obtained from theoretical calculations and experimental observations was the same. Therefore, it is still valid to utilize fitting results to predict the mechanical strength of BOAC structures.

4.4 Discussion on nanoindentation and bondability test

From the previous section, we knew that the composite BOAC substrate was not a uniform substrate, but exhibited a continually changing substrate with increasing indenter depth. A simplified approach based on King's model was employed to quantify the mechanical strength of BOAC structures, assuming that the composite BOAC substrate was a uniform substrate. Although the exact values of the composite BOAC substrate cannot be extracted, we still could use the quantified values based on King's model to predict the BOAC structures because the tendency of mechanical strength from nanoindentation results was the same with the theoretical calculations.

One of the purposes of this study outlined in Chapter 2 is to establish a success criterion of minimum required mechanical strength without bondability failure. The bondability test included wire pull, ball shear and cractering test, PU: K&S. The test bonding parameter was the same with typical and major boning condition. The Min. Force ^{Spec} (wire pull, ball shear) which defined by assembly house was a criterion to distinguish which BOAC structures would pass the bondability test. For all the BOAC structures including the one with the weakest ULK dielectrics (65ULKBOAC), the Min. Force (wire pull, ball shear) $\geqq$ Min. Force ^{Spec} (wire pull, ball shear). They all passed bondability tests carried out in UMC. So far, the novel nanoindentation test can distinguish and analyze the mechanical strength of BOAC structures. But, it is still not feasible to set minimum criteria of mechanical strength for BOAC structure to pass bondability test because none of BOAC structure in this study fails. In order to correlate between the bondability and nanoindentation test, a negative control BOAC structure with bondability failure will be designed and validated in future research. Nevertheless, BOAC structure with the weakest mechanical support in this study (65ULKBOAC) has a modulus of 70 GPa in composite substrate, which can be

considered as a sufficient condition for any new BOAC layouts and designs to pass the bondability test.

Chapter 5 Conclusions

In this thesis, a quick turn-around, experimental methodology based on nanoindentation has been successfully developed to accelerate the evaluation of various BOAC layout designs without a full array of reliability tests. Nanoindentation, which simulated the impact force of wire bonding (down force of 5~25 mN), was adopted to characterize mechanical resistance of BOAC structures, which consisted of oxide/multi-layered copper/low-k structures below Al bond pad, as a function of indenter depth by means of substrate effect. The mechanical stiffness of BOAC structures could be quantified using King's model assuming a uniform two-layered Al/substrate system and correlated with their bondability results.

Four parameters affecting the mechanical strength of BOAC such as bond pad types, copper density, line width/pitch (technology nodes) and low-k materials were investigated in this thesis to identify general design rules for BOAC layouts and structures. In the bond pad design, normal pad possessed much stronger mechanical support than BOAC pad because normal pads had full array of dummified trench/via reinforcement in M1-6, while BOAC structures had only sparse vias (< 6 %) randomly layout in M1-6.

For BOAC structures with different copper density and layout (block copper vs. ring copper) in the top metal layer, metal density had little influence on the mechanical strength of BOAC structures. This indicated that the top Al pad (1.2 μm) and oxide layer (1.2 μm) absorbed the majority of impact force; thus provided good protection for the structures underneath the top Al pad and oxide layer.

When the metal line widths and pitches scaled from 90 nm to 65 nm process node, the modulus of composite substrate, E_{cs} in 65 nm parts was larger because the Cu fractions in M1-6 layer were higher by increased aspect ratio of copper in 65 nm node.

The type of low-k materials was found to have great influence on the mechanical strength of BOAC structures. E_{cs} of ultra low-k parts was much lower than E_{cs} for BOAC with low-k due to low modulus of ultra low-k and its weak interfacial adhesion. Care and consideration of weak modulus, and more importantly the interfacial adhesion shall be taken to avoid mechanical reliability or device failure when ultra low-k materials are chosen as the ILD materials. In summary, BOAC structures can be strengthened by (1) adding a stronger buffer layer such as oxide layer on the top of BOAC structures, (2) increasing aspect ratio (AR) in Cu/low-k layer, and (3) using low-k materials with better modulus and interface adhesion.

Different BOAC stacks were also investigated in this thesis. The first BOAC structure was Al/composite substrate system which could be categorized as a soft film/hard substrate system. The other BOAC structure was oxide/composite substrate system which could be categorized as a hard film/soft substrate system. The objective was to cross-check the fitting results based on King's model and to understand any difference in the values obtained by nanoindentation method. The results showed that the E_{cs} of oxide film/composite substrate were lower than those of Al film/composite substrates for the same BOAC design because the affected region within the composite substrates changed with increasing indenter depth during nanoindentation. Moreover, the results also indicated that the hardness would affect the modulus in the nanoindentation measurement. For Al film/composite substrate system, the E_{cs} was overestimated because the contact area (A) was underestimated. For the oxide film/composite substrate, the E_{cs} was underestimated because the contact area (A) was overestimated.

Then P/S^2 term was then used to eliminate the contact area effect from nanoindentation in order to study the true modulus behavior during indentation. The results truthfully showed a varying multilayered substrate with increasing indenter

depth. This method could be used to analyze the changing mechanical strength of multilayer in BOAC structures as a function of indenter depth. A 3-layered model based on Al/oxide/soft composite substrate was used to estimate the mechanical strength of BOAC structures under oxide layer by using (1) experimental observations, which used P/S^2 to exclude hardness effect and (2) theoretical calculations, which used the equation of composite materials. From the results, we found the values from the equation of composite material E_r were lower than those observed in experiments. The lower values in theoretical values may be due to the underestimation of contribution from top harder layer in soft composite substrate such as Cu/FSG and the strain-hardening induced by the Cu in copper/low-k layers. Moreover, the theoretical calculation cannot take weak adhesion due to porosity into account. The P/S^2 (experimental observations) results showed not only the same tendency of mechanical strength as that of theoretical calculation using the equation of composite materials, but also smaller deviation from theoretical calculation, as compared to values obtained from King's model fitting. A modification of King's model will be needed if the exact modulus of the multi-layered substrates is sought after.

Overall, a novel methodology based on nanoindentation has been successfully established to distinguish the mechanical strength of various BOAC structures through a composite modulus values using a simplified film/uniform substrate model or P/S^2 model. Unfortunately the BOAC structures in this thesis were all passing the bondability test. Nevertheless, a modulus of 70 GPa in composite substrate of bond pad structure based on King's model fitting results, can be considered as a sufficient condition for new BOAC layouts meeting the bondability tests.

Reference

[1] International Technology Roadmap for Semiconductors, executive summary (2005).

[2] G. Heinen, R. J. Stierman, D. Edwards, and L. W. Nye, IEEE Proc. of 44th ECTC, 922 (1994).

[3] K. M. Chen B. C. Wu, K. H. Tang, F. Y. Cheng, N. H. Kao, and J. Y. Lai, Microelectronics Reliability, **46**, 335 (2006).

[4] B. Halg, IEEE Micro Electro Mechanical Systems Workshop, 172 (Feb 1990).

[5] L. Shen and K. Zeng, Microelectronic Engineering, **71**, 221 (2004).

[6] Y. Liu, D. Desbiens, S. Irving, and T. Luk, IEEE Proc. of 55th ECTC, 861 (2005).

[7] Y. Liu, S. Irving, and T. Luk, IEEE Proc. of 54th ECTC, 383 (2004).

[8] 呂宗興, 電子構裝技術的發展歷程, 工業材料 (1997).

[9] 鐘文仁, 陳佑任, IC 封裝製程與 CAE 應用 (2005).

[10] International Technology Roadmap for Semiconductors, executive summary (2006).

[11] G. G. Harman, Wire Bonding in Microelectronics Materials, Processes, Reliability, and Yield (second ed.), McGraw-Hill (1997).

[12] R. Singh, and R. K. Ulrich, The Electrochemical Society Interface, **8 (2)**, 26 (1999).

[13] M. T. Bohr, IEEE International Electronic Device Meeting, 241 (1995).

[14] D. Edelstein, J. Heidenreich, R. Goldblatt, W. Cote, C. Uzoh, N. Lustig, P. Roper, T. Mcdevittt, W. Motsifft, A. Simon, J. Dukovic, R. Wachnik, H. Rathore, R. Schulz , L. Su, S. Lucet, and J. Slatteryt, IEEE International Electronic Device Meeting, 773 (1997).

[15] 楊正杰, 張鼎張, 鄭晃忠, 銅金屬與低介電常數材料與製程, 毫微米通訊 **7**, 40.

[16] J. Leu, Low-k Materials and Processing Thchnologies Class (2006).

[17] K. Mikagi, N. Ishikawa, T. Usami, M. Suzuki, K. Inoue, N. Oda, S. Chikaki, I. Sakai, and T. Kikkawa, IEEE International Electronic Device Meeting, 365 (1996).

[18] S. J. Martin, J. P. Godschalx, M. E. Mills, E. O. Shaffer, and P.H. Townsend, Adv. Mater., **12**, 1769 (2000).

[19] H. J. Lee, E. K. Lin, H. Wang, W. L. Wu, W. Chen, and E. S. Moyer, Chem. Mater., **14**, 1845 (2002).

[20] J. H. Zhao, I. Malik, T. Ryan, E. T. Ogawa, and P. S. Ho, APPLIED PHYSICS LETTERS, **74**, 944 (1999).

[21] S. Allada, "Low K Adhesion Issues in Cu/Low K Integration", IEEE (1999).

[22] J. B. VELLA, I. S. ADHIHETTY, K. JUNKER, and A. A. VOLINSKY, International Journal of Fracture, 119/120, 487 (2003).

[23] K. Y. Chou, M. J. Chen, and C. W. Liu, IEEE Trans. Electron Dev., **49**, 2279 (2002).

[24] K. J. Hess, S. H. Downey, G. B. Hall, T. Lee, L. L. Mercado, J. W. Miller, W. C. Ng, and D. G. Wontor, IEEE Proc. Of 53th ECTC., 1344, 2003.

[25] B. Chandran, R. Mahajan, M. Bohr, C. H. Jan, Q. T. Vu, "The Mechanical Side of Ultra-Low k: Can it Take the Strain?", Future Fab Intl., 17 (2004).

[26] D. Degryse, B. Vandevelde, and E. Beyne, IEEE TRANSACTIONS ON COMPONENTS AND PACKAGING TECHNOLOGIES, **27,** *4* (2004).

[27] O. van der Sluis, R. A. B. Engelen, W. D. van Driel, M. A. J. van GiIs, and R. B. R. van Silfhout, 7th. Int. Conf: on Thermal, Mechanical and Multiphysics Simulation and Experiments in Micro-Electronics and Micro-Systems,

EuroSimE (2006).

[28] D. Tabor, The hardness of metals., Oxford: Oxford Univ. Press (1951).

[29] I. N. Sneddon, The relaxation between load and penetration in the axisymmetric Bussinesq problem for a punch of arbitrary profile.

[30] G. M. Pharr, and W. C. Oliver, J. Mater. Res., **4**, 94 (1989).

[31] W. C. Oliver and G. M. Pharr, J. Mater. Res., **7**, 1564 (1992).

[32] A. A. Volinsky, J. B. Vella, and W. W. Gerberich, Thin Solid Films, **429**, 201 (2003).

[33] A. K. Bhattacharya and W. D. Nix, International Journal of Solids and Structures, **24**, 1287 (1988).

[34] R. B. King, Int. J. Solids Struct., **23**, 1657 (1987).

[35] B. A. Walmsley, et al., Journal Applied Physics, **98**, 044904 (2005).

[36] R. Saha and W. D. Nix, Acta. Mater., **50**, 23 (2002).

[37] J. Vitiello, A. Fuchsmann, L. L. Chapelon, V. Arnal, D. Barbier, and J. Torres, Microelectronic Engineering, **82**, 422 (2005).

[38] S. Chen, L. Liu, and T. Wang, Surf. Coat. Technol., **191**, 25 (2005).